CHAPTER IV

Neurotrophic potency and mechanism of neuroprotective action of snake venom-nerve growth factors-derived custom peptides in pheochromocytoma of the rat adrenal medulla (PC-12) cells

4.1 Results

4.1.1 The biophysical characterization to ascertain the purity of the synthesized peptides

HPLC chromatograms showed the purity of the synthetic peptides (single peaks within 8-12 min of retention time) and the scrambled peptide (Figs 4.1A-C). The ESI-mass spectrometry analysis also suggested the purity of the peptide preparations (Figs 4.1D-F). The CD spectrum of custom peptide TNP revealed that it was composed of α-helices (37.6%), random coils (30.9%), and turns (31.5%) with a characteristic minimum absorbance at 210 nm (Fig 4.2A). The analysis of the CD spectrum of custom peptide HNP revealed that it was mainly composed of turns (100%) with characteristic maximum absorbances at 202 and 224 nm (Fig 4.2B). The CD spectrum of scrambled peptide also revealed that it was mainly composed of turns (100%) with characteristic maximum absorbances at 202 and 224 nm (Fig 4.2C).

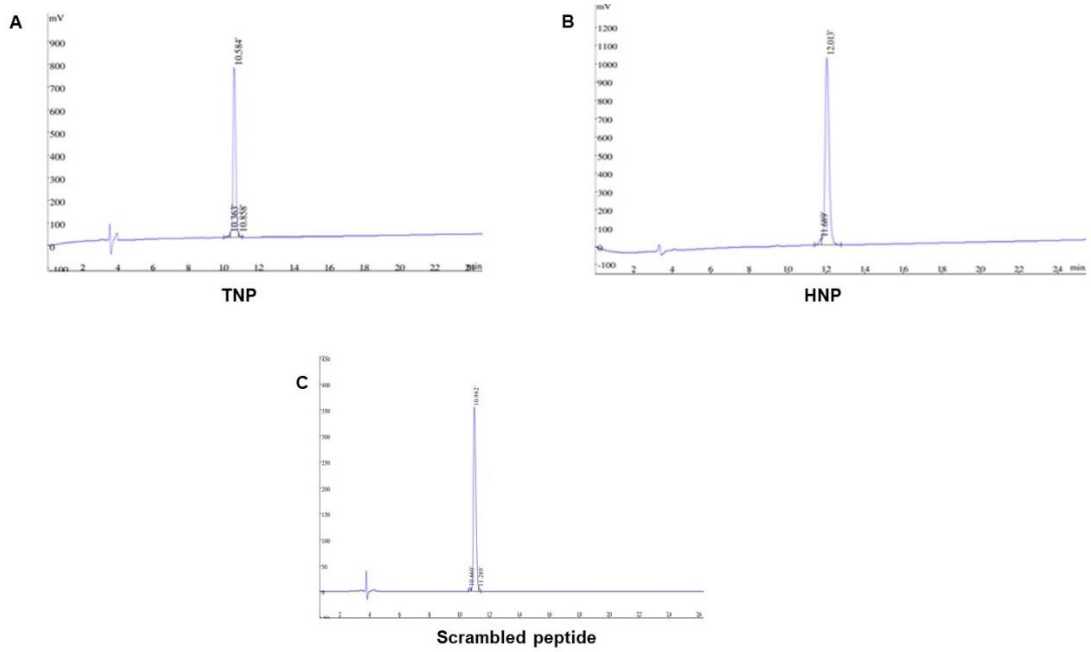

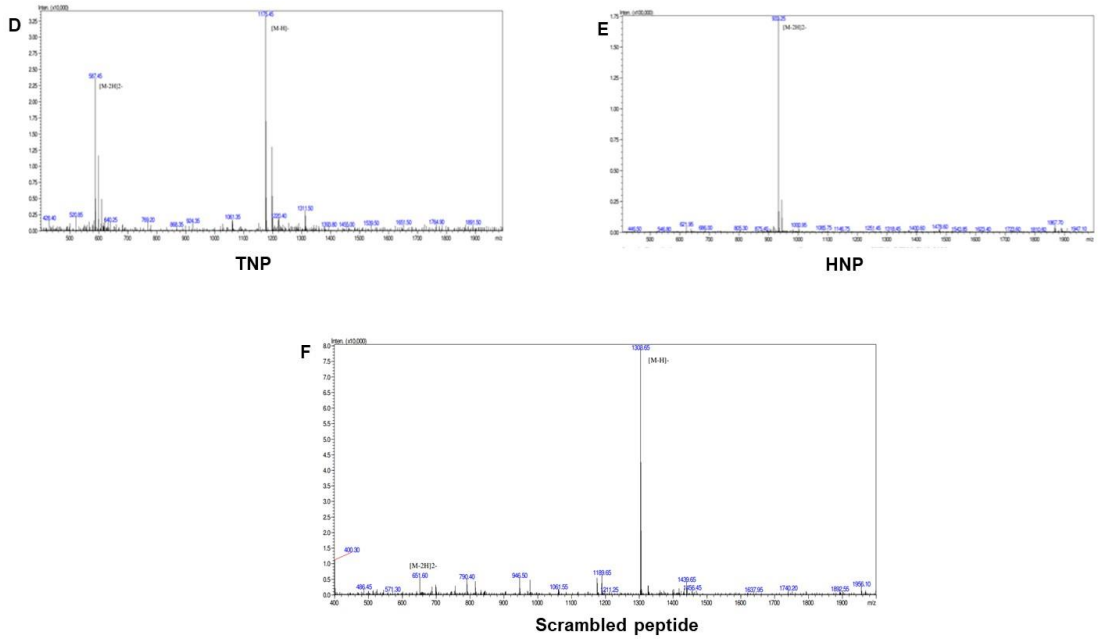

Fig 4.1 HPLC chromatogram of the custom peptide (A) TNP, (B) HNP, and (C) Scrambled peptide. MS/MS spectrum of the peptide (D) TNP, (E) HNP, and (F) Scrambled peptide was analysed by ESI LC/MS-MS.

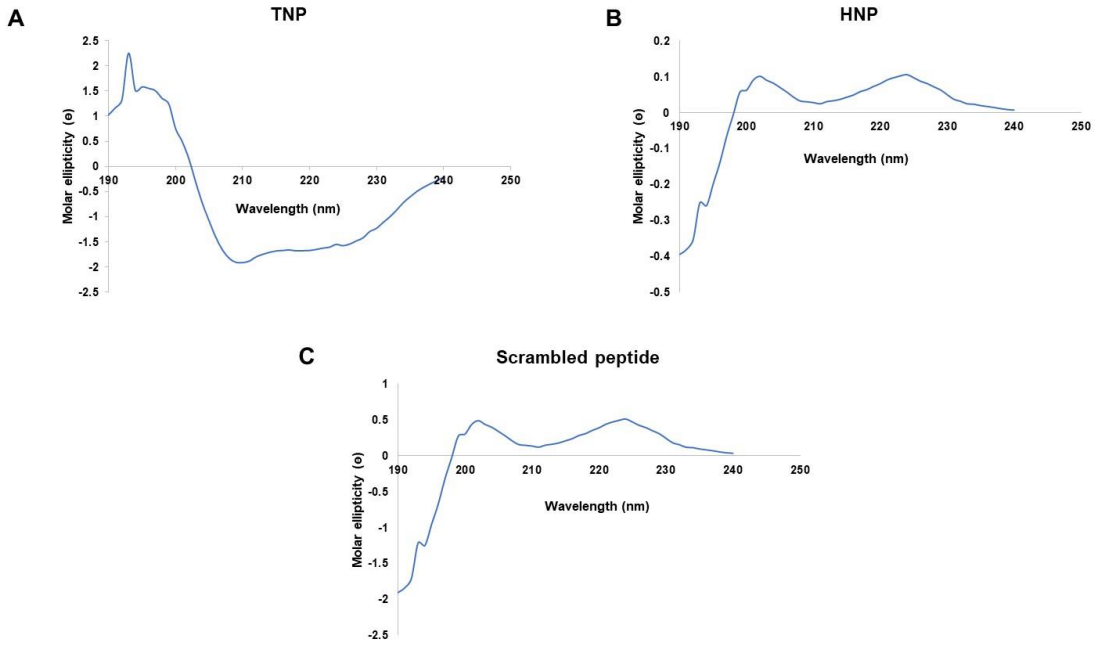

Fig 4.2 Circular dichroism (CD) spectra of custom peptides (A) TNP, (B) HNP, and (C) Scrambled peptide. Custom peptides/Scrambled peptide (0.3 mg/ml) were dissolved in 20 mM potassium phosphate buffer pH 7.0 and the far UV-CD spectra were recorded at

room temperature (~25 °C) between 190 and 250 nm against the appropriate buffer (blank).

4.1.2 Computation analysis to predict the interaction between different domains of TrKA receptor and SV NGF-derived custom peptides

The sequence and biophysical properties of the TrkA receptor-binding custom peptides (TNP and HNP) and the scrambled peptide are summarized in Table 4.1. Different domains of human TrkA were obtained from the PDB structures (Fig 4.3A). Domain-3 of TrkA was characterized as an NGF-binding domain site (in humans) (Fig 4.3A). Molecular docking revealed a high-affinity binding that formed a complex between the peptides (TNP and HNP) and TrkA domain-3 (Figs 4.3B-C). Glide docking scores were found to be -9.35 (TNP) and -5.54 (HNP), and similarly, the MMGBSA binding energies (docked complex) were found to be -77.77 (TNP) and -68.03 (HNP) kcal/mol (Table 4.2). However, *in silico* analysis revealed that scrambled peptide does not form a stable complex with the human TrkA receptor (Fig 4.3D). The glide docking score of the scrambled peptide was found to be -9.99 and the MMGBSA binding energies (docked complex) were found to be -60.99 kcal/mol (Table 4.2).

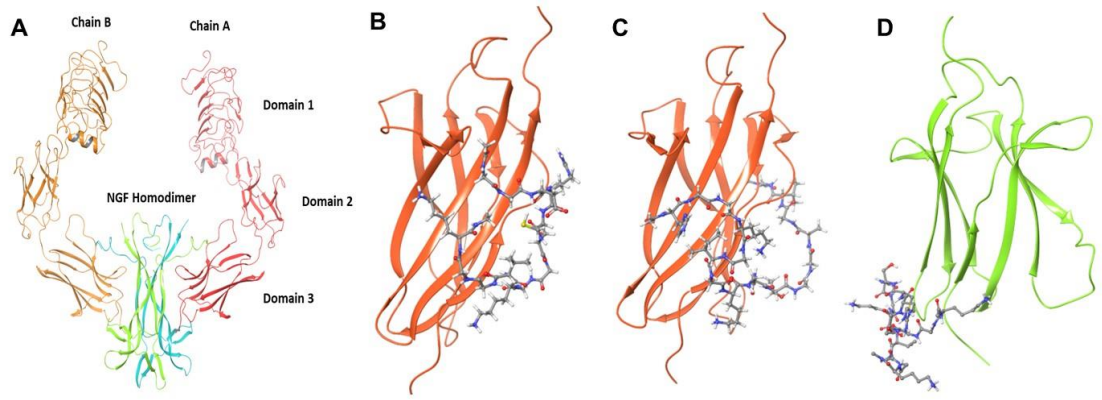

Fig. 4.3 The *in silico* analysis of (A) Human TrkA receptor Chain A and B in complex with human NGF homodimer (PDB ID- 2IFG). The 3D model shows the interaction of TrkA with (B) TNP, and (C) HNP (D) Scrambled peptide to form a ligand-receptor complex. The ball and stick structure represent peptide structure, and the string model corresponds to TrkA receptor domain-3.

Table 4.1 The custom peptide and scrambled peptide sequences and their properties

Peptide	Peptide sequence	Length (amino acid)	Molecular weight (kDa)	Solubility	Extinction coefficient (M^{-1} cm^{-1})	Isoelectric point (pH)	Purity (RP-HPLC analysis)	Hydrophobicity (Kcal * mol^{-1})
TNP	NH_2-GGDRCSGGKVGGK-COOH	13	1.2	DMSO (0.1% w/v)	0	9.67	98%	+25.83
HNP	NH_2-HGGKGIGKGGTGGAGVG-COOH	17	1.4	DMSO (0.1% w/v)	0	10.65	98%	+26.50
Scrambled peptide	NH_2-KGGDRCSGGAVGVK-COOH	14	1.3	DMSO (0.1% w/v)	0	10.28	98%	+28.63

Table 4.2 Glide scores and molecular mechanics/generalized Born surface area (MM/GBSA) binding energy of custom peptides with domain 3 of human TrkA.

Custom peptide	Glide docking score	MMGBSA binding energy (ΔG) (kcal/mol)	MMGBSA binding energy (ΔG) after simulation (kcal/mol)
TNP	-9.35	-77.77	-93.65
HNP	-5.54	-68.33	-106.99
Scrambled peptide	-9.99	-60.99	-40.54

The stability of the docked domain-3 with the TNP/ HNP complex was studied using molecular dynamic simulations for 300 ns. In all cases, the RMSD of the TrkA domain-3 backbone was found to be stable over the simulation trajectory. For TNP, the first 25 - 50 ns of simulation showed a higher variation in RMSD with a stable complex forming afterward (Fig 4.4A). Unlike the molecular docking results, the molecular dynamic simulations predicted a stable complex of HNP with domain-3 of TrkA (Fig 4.4B), and the average MMGBSA binding energy of TNP and HNP were -93.652 and -106.998 kcal/mol, respectively. However, high RMS deviation was observed up to 300 ns of simulation for scrambled peptide (Fig 4.4C), and the average MMBGBSA binding energy of scrambled peptide was -40.54 kcal/mol.

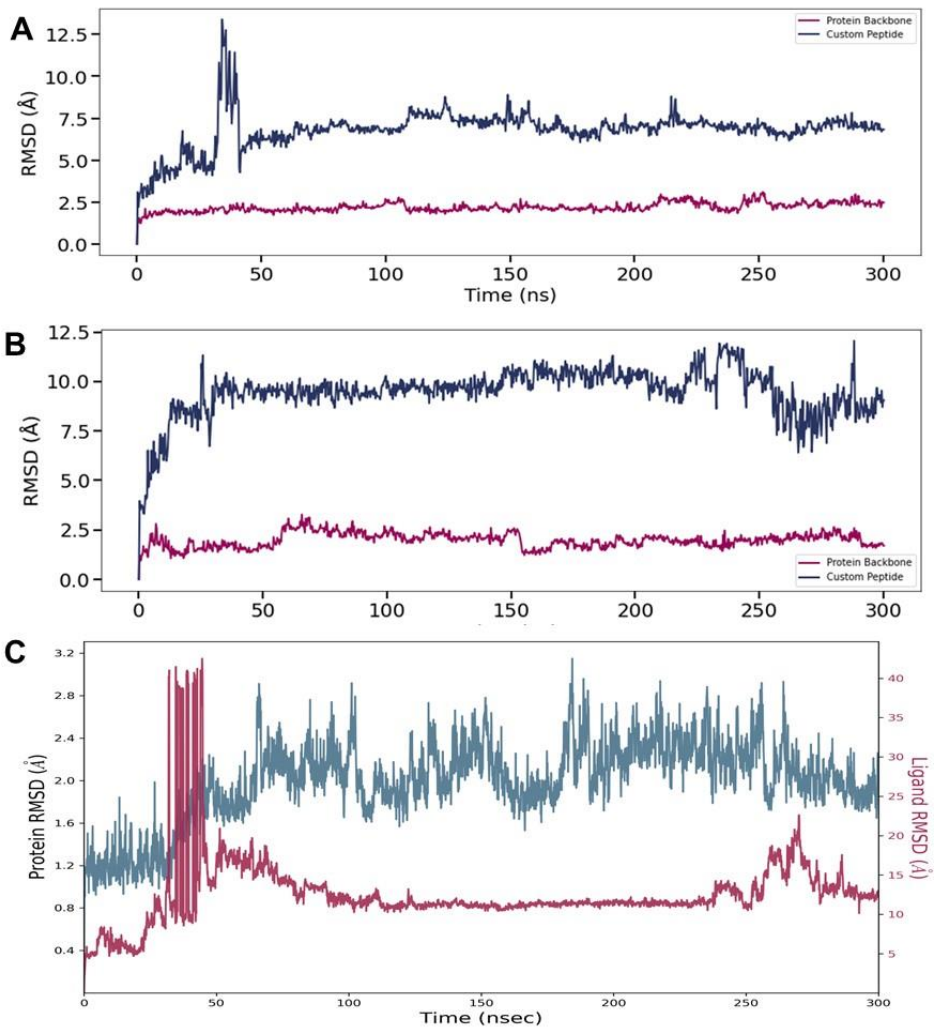

Fig 4.4 Molecular dynamic simulation of domain-3 backbone and custom peptides (A) TNP, (B) HNP, and (C) Scrambled peptide shown in an RMSD (root mean square deviation) plot throughout the simulation trajectory for 300 ns.

TNP interacted with five different amino acid residues of TrkA domain-3, and the interaction was stable up to 87% of the simulation time (Fig 4.5A). The major TrkA domain-3 residues Arg273, Ser277, and Val198 participated in the interaction with Asp3, Gly11, and Gly12 TNP residues, respectively, and Glu275 of domain-3 interacted with Arg4, Cys5, and Ser6 of TNP (Fig 4.5A). Nevertheless, HNP demonstrated the highest degree of stable interaction (i.e., up to 62% of the time) with seven different amino acid residues of TrkA domain-3 (Fig 4.5B). The major TrkA domain-3 residue Ser371 interacted with His1, Gly2, and Lys8 residues of HNP. Leu290 of domain-3 interacted with Gly13 and Gly15 of TNP and the other domain-3 residues (Ala363, Ala370, Ser373,

His291, and Ser304) participated in the interaction with HNP residues Ile6, Ile6, Thr11, Ala14, and Val16, respectively (Fig 4.5B).

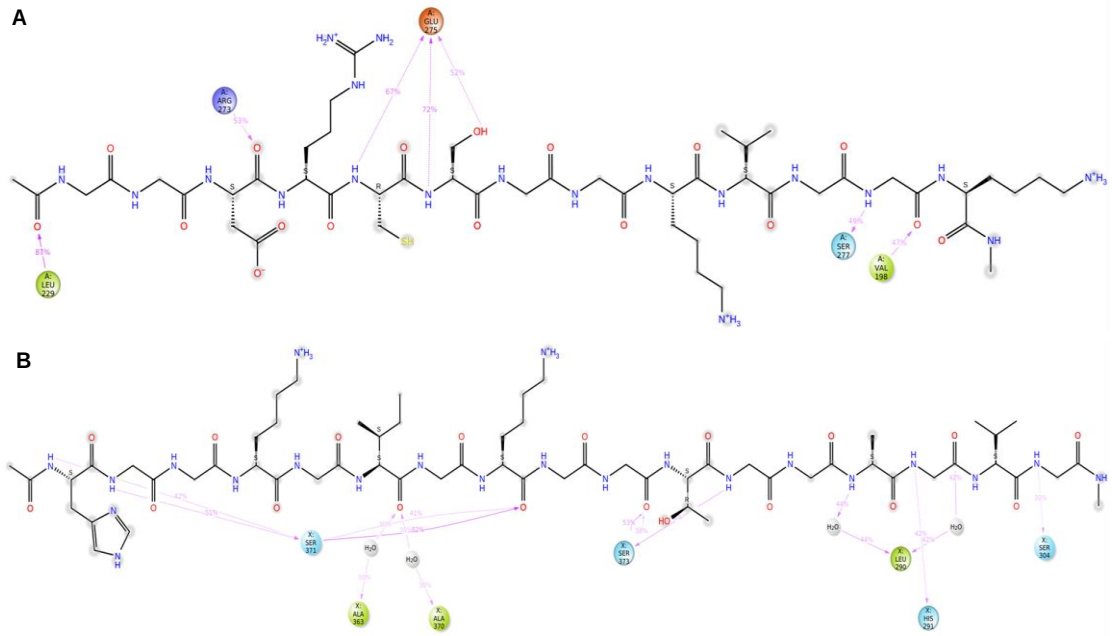

Fig 4.5 Schematic diagram depicting the interaction of custom peptides (A) TNP (B) HNP with domain-3 of the TrkA receptor. The percentage of interaction is shown in the figure recorded over the simulation time of 300ns.

4.1.3 The FITC-conjugated custom peptides showed exclusive binding to mammalian cells expressing the TrkA receptor but not to cells with TrkB or TrkC receptors

The spectrofluorometric analysis of FITC-custom peptides (TNP and HNP) but not the scrambled peptide showed a significant binding in a time-dependent manner to the TrkA receptor expressed in MCF7, MDA-MB-231, and PC-12 cells but not to L6 cells (devoid of extracellular TrkA receptors) (Fig 4.6A). The fluorescence intensity was significantly higher (3 to 30-fold increase) in HNP and TNP-treated samples compared to the control L6 cells. In any case, the binding efficacy of the HNP peptide was significantly higher ($p \leq 0.05$) for MCF7 and PC-12 cells, compared to those of the TNP peptide. For the MDA-MB-231 cells, no significant difference was seen between the two peptides up to 60 min of incubation (Fig 4.6A).

The FITC-conjugated peptides also showed a significant increase ($p \leq 0.05$) in binding efficacies to PC-12 cells in a concentration-dependent manner (from 50 to 1000 ng/mL, equivalent to 40 to 800 nM) (Fig 4.6B). The binding affinity (Kd value) of TNP and HNP towards the PC-12 cell line was determined at 1.03 x 10^{-7} and 0.80 x 10^{-7} M, respectively (Fig 4.6C).

The binding of FITC-custom peptides to MCF-7 (Fig 4.6D), and MDA-MB-231 (Fig 4.6E) cells expressing TrkA receptor was evident by fluorescence microscopic analysis; however, no fluorescence signal was detected in L6 cells post incubation with FITC-conjugated peptides (Fig 4.6F).

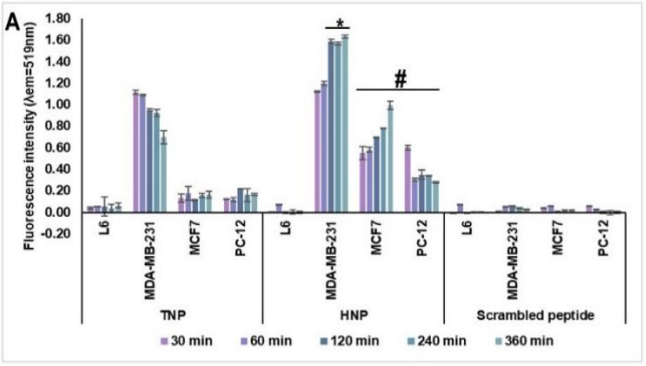

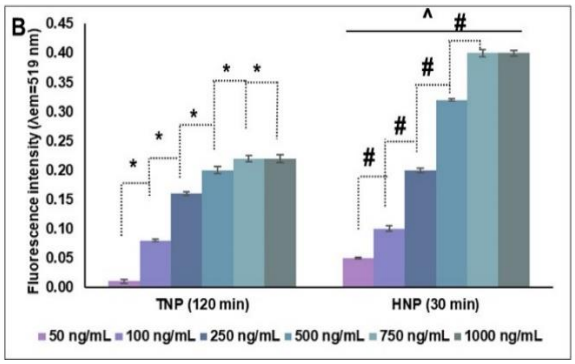

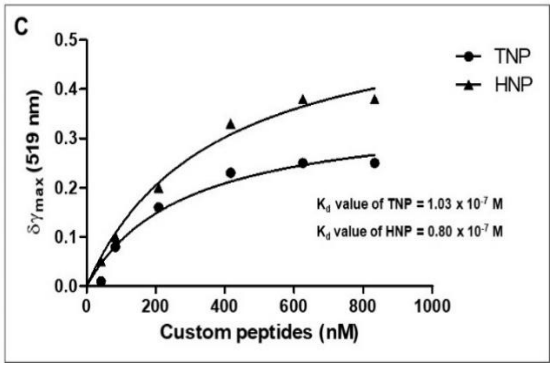

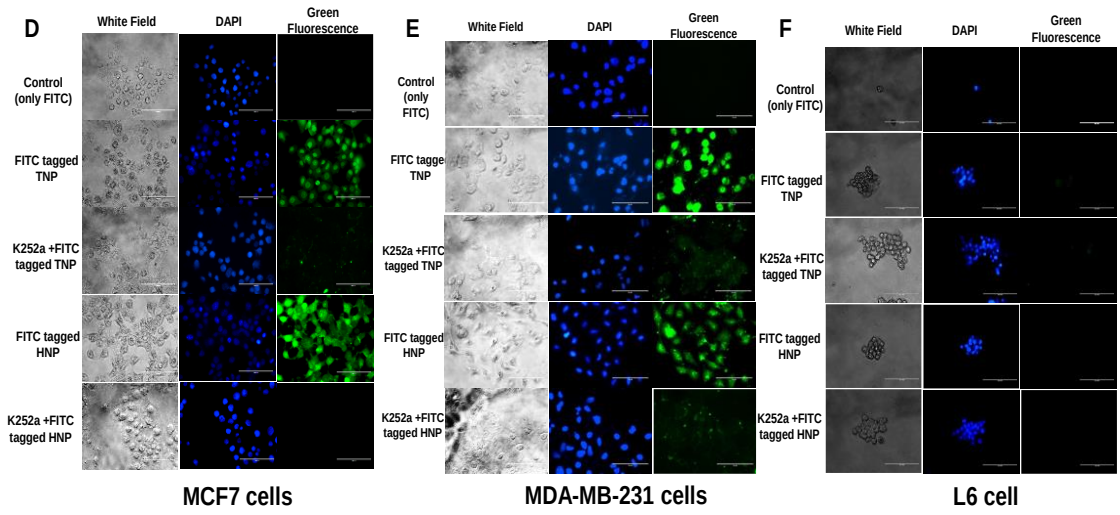

Fig 4.6 Fluorescence analysis to determine the (A) time-dependent binding (30 min to 360 min) of custom peptides (100 ng/mL, ~71nM) with the TrkA receptor of cells. L6 cells (non-TrkA expressing cells) were taken as control. Significance of difference in the binding of TNP (for 120 min to 360 min) with respect to HNP for MDA-MB-231, $^{*}p < 0.05$. Significance of difference in the binding of TNP (for 30 min to 360 min) with respect to HNP for MCF7 and PC-12 cell line, $^{\#}p < 0.05$. (B) Binding of custom peptides with cell surface TrkA receptor of PC-12 cells in an increasing concentration of custom peptides (50 ng/mL to 1000 ng/ml, equivalent to 40 to 800 nM). Significance of difference in the binding between different concentrations for TNP $^{*}p < 0.05$ and for HNP $^{\#}p < 0.05$. Significance of difference in the binding of TNP with respect to HNP, $^{\wedge}p< 0.05$. (C) A hyperbola curve was plotted for change in λmax (Δλmax) against the concentrations (nM) of the custom peptide with TrkA receptor expressing PC-12 cells (1 x 10^4 cells) and the Kd value was determined using GraphPad Prism 8.1.1 software. The binding of FITC-custom peptide (100 ng/mL) with (D) MCF7, (E) MDA-MB-231, and (F) L6 cells was observed under fluorescence. The binding of custom peptides was also shown in the presence or absence of a chemical inhibitor of the Trk family (K252a). Magnification was 40X. Values are mean ± SD of triplicate determinations.

4.1.4 Custom peptide-induced neurite outgrowth and differentiation of PC-12 cells

The TNP and HNP did not demonstrate *in vitro* cell cytotoxicity (Figs 4.7A-B) and showed negligible haemolytic, platelet-modulating, and plasma-clotting activities (Table 4.3).

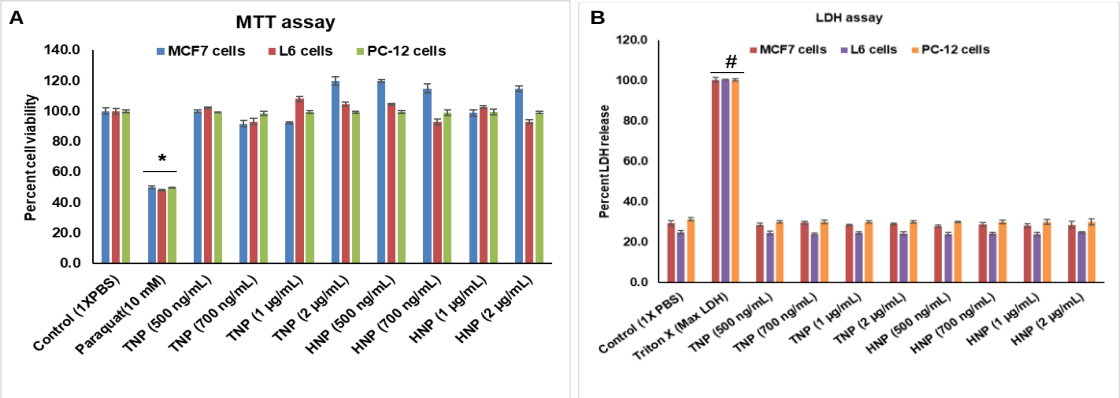

Fig 4.7 Concentration-dependent *in vitro* cytotoxicity of synthetic peptides (TNP and HNP) and PT (10 mM, positive control) against mammalian cells. The cells were incubated with progressive concentrations of custom peptides (500 ng/mL to 2 µg/mL) with mammalian cells (MCF7, PC-12, and L6 cells) at 37°C in a CO_2 incubator for 24h. Determination of cytotoxicity by (A) MTT assay, and (B) LDH release assay. Significance of difference in the cell viability by MTT assay for paraquat-treated cells with respected TNP and HNP treated cells, $^{*}p < 0.05$. Significance of difference in the cell viability by LDH release assay for Triton-X treated cells with respect to TNP and HNP treated cells, $^{\#}p < 0.05$. Values are mean ± SD of triplicate determinations.

Table 4.3 *In vitro* effect of custom peptides on mammalian blood

Custom peptides	**[a]Plasma clotting activity (sec),**	**Coagulant (C) anticoagulant (AC)**	**[b]Platelet aggregation (%)**	**[c]Indirect hemolysis (%)**
NTP	10.6 ± 0.14	C	(-) 2.9± 0.9	0.39± 0.04
HTP	5.7 ± 0.11	C	(+) 3.1± 0.7	0.33± 0.05

[a] Plasma clotting activity of custom peptide (TNP, and HNP) was assayed with 300 µL of goat platelet-poor plasma (PPP) at a dose of 5 µg/mL. The clotting time of untreated plasma was 120 sec. Values are mean ± SD of triplicate determinations. [b]Platelet aggregation property of custom peptides (TNP, and HNP) was assayed against goat platelet-rich plasma (PRP) at a dose of 1 µg/mL. (+) and (−) represent platelet aggregation and deaggregation activities, respectively. [c]The Hemolytic activity of custom peptides (TNP, and HNP) was assayed against 5% (v/v) mammalian erythrocytes at a dose of 1 µg/mL.

Phase-contrast microscopic images of neurite outgrowth in PC-12 cells 14 days post-treatment with custom peptides are shown in Figs 4.8A-H. The average neurite length (µm) is represented by the box and whisker plot, which shows the variation for the different concentrations (12.5 to 100 ng/mL, equivalent to 18 to 71 nM) of peptide (TNP

and HNP), compared to mouse 2.5S NGF (Positive control) (Fig 4.8I). Custom peptides TNP, HNP, and mouse 2.5S-NGF induced neurite outgrowth and differentiation in PC-12 cells to different extents (Figs 4.8I-J). The custom peptides showed significant neurite outgrowth at a minimum concentration of 50 ng/mL (equivalent to 36 nM). The average neurite length, and the percentage of differentiated cells, were significantly higher ($p \leq 0.05$) for TNP and HNP at the same concentration (100 ng/mL, equivalent to 71 nM), compared to mouse 2.5S-NGF (positive control); however, no significant difference ($p>0.05$) was observed between the TNP and HNP peptides.

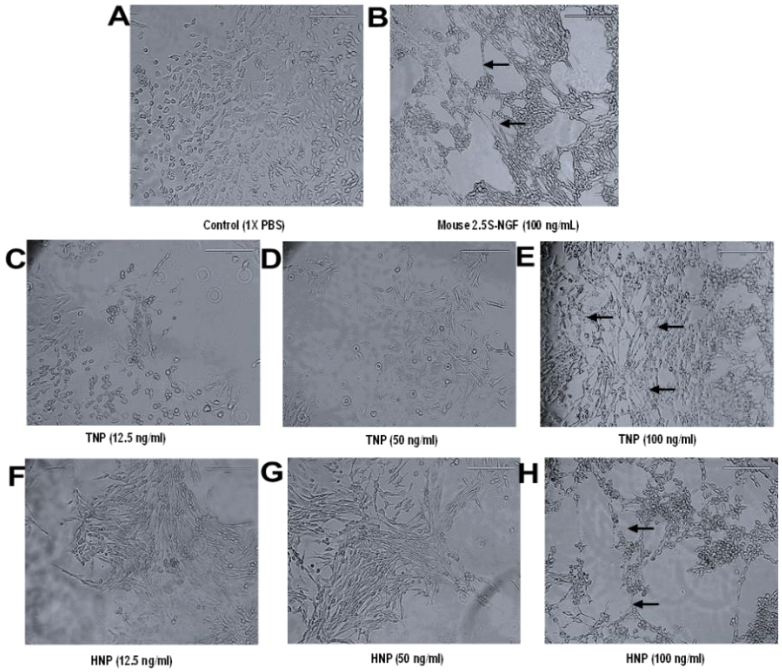

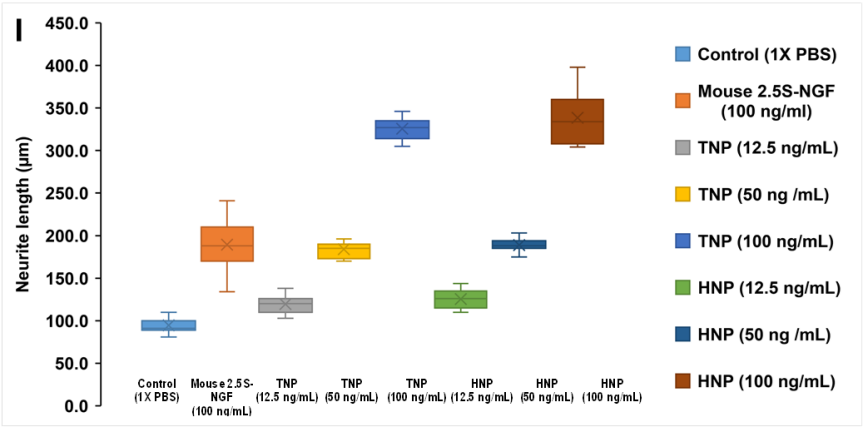

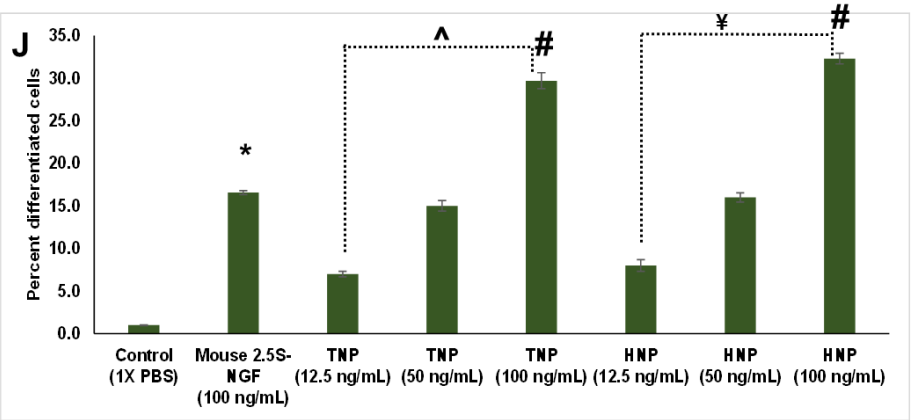

Fig 4.8 Concentration-dependent (12.5 to 100 ng/mL) determination of neurite outgrowth in rat pheochromocytoma (PC-12) cells treated with custom peptides (TNP & HNP) post 14 days of incubation at 37°C, 5% CO_2. The cells were observed under a phase-contrast microscope at 20x magnification. The appearance of neurite outgrowth from PC-12 cells is indicated by black arrows. (A) 1X PBS (control) treated cells, (B) mouse 2.5S-NGF treated cells, (C-E) TNP-treated cells with different concentrations (12.5 to 100 ng/mL), (F-H) HNP-treated cells with different concentrations (12.5 to 100 ng/mL). (I) Box and whisker plots represent average neurite outgrowth per cell (in µm). (J) Bar graph showing the percentage of differentiated cells (total number of cells showing neurite outgrowth) in custom peptide and mouse 2.5 S-NGF-treated PC-12 cells. The neurite length was determined using MOTIC IMAGE PLUS 3.0 software. Significance of difference in the controls with respect to mouse 2.5S-NGF, $^{*}p < 0.05$. Significance of difference in mouse 2.5S-NGF with respect to TNP and HNP (at the concentration 100 ng/mL), $^{\#}p < 0.05$. Significance of difference in different concentrations for TNP, $^{\wedge}p < 0.05$ and for HNP, $^{¥}p < 0.05$. Values are mean ± SD of triplicate determinations.

4.1.5 Chemical inhibition of TrkA receptor (K252a), PI3K/AKT (LY294002), and MAPK/ERK (U0126) pathways inhibited neuritogenesis induced by the custom peptides in PC-12 cells

The percentage of cell differentiation was examined for PC-12 cells treated with custom peptides that were pre-incubated with or without chemical inhibitors, after 14 days of incubation. The results show that the potency of the custom peptides in inducing neurite outgrowth and cell differentiation activities was significantly inhibited ($p \leq 0.05$) by the three chemical inhibitors (K252a, LY294002, and U0126) (Fig 4.9A). The

inhibition in the differentiation of PC-12 cells by peptides (100 ng/mL, equivalent to ~71 nM) in the presence or absence of chemical inhibitors were ranked in descending order MAPK/ERK (U0126) pathway inhibitors (15 to 16% decrease) > PI3K/AKT (LY294002) (12 to 13 % decrease) > TrkA receptor inhibitor (K252a) (9 to 10% decrease) when compared to neurite outgrowth and cell differentiation activities of custom peptides without inhibitor. These findings corroborate well with our earlier findings with NGFs from Indian Russell's viper and Indian cobra venoms [1-3].

The blocking of the TrkA receptor significantly inhibited ($p \leq 0.05$) differentiation of PC-12 cells by TNP and HNP, while blocking of the TrkB and TrkC receptors with their respective antibodies did not affect differentiation of the PC-12 cells (Fig 4.9B). Thus, the peptides appear to bind exclusively to TrkA receptors.

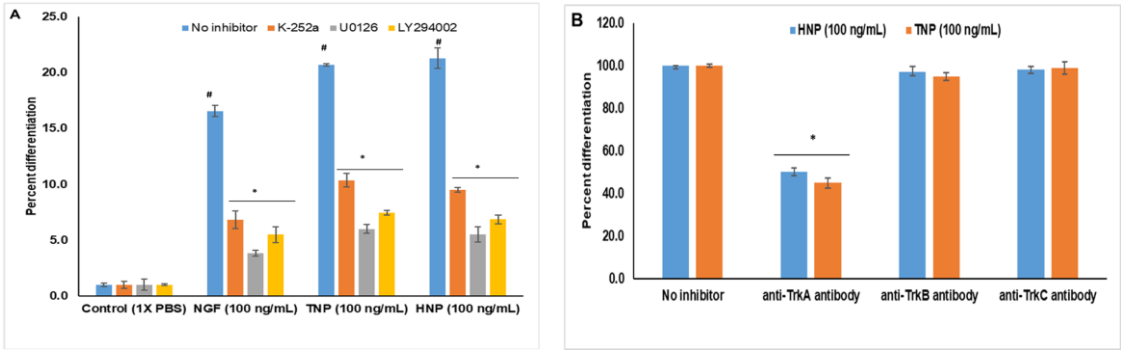

Fig 4.9 (A) Effect of small synthetic inhibitors of major signaling pathways on neuritogenesis potency of custom peptides (TNP, and HNP, 100 ng/mL equivalent to 71nM), and NGF (positive control, 100 ng/mL) in PC-12 cells. Significance of difference in the percent differentiation of control cells compared to NGF, TNP, and HNP when no inhibitor was added, $^{\#}p \leq 0.05$. Significance of difference in the percent cell differentiation between with inhibitors (K-252a, U0126, and LY294002) and without inhibitors, $^{\#}p \leq 0.05$ (B) Effect of anti-TrkA, TrkB, TrkC antibody (1:1000) on neuritogenesis potency of custom peptides (TNP, and HNP, 100 ng/mL equivalent to 71nM), and NGF (positive control) in PC-12 cells. Significance of difference in the percent cell differentiation between with anti-TrkA antibody and without inhibitors, $^{*}p \leq 0.05$. Values are mean ± SD of triplicate determinations.

4.1.6 Pre-treatment of PC-12 cells with custom peptides enhanced their cell survival against PT-induced cell death

Pre-treatment of PC-12 cells with TNP and HNP (100 ng/mL, ~71 nM) demonstrated a significant 27 to 30% increase ($p \leq 0.05$) in their percent cell viability against PT (10 mM, IC_{50})-induced cell death, compared PC-12 cells that had only been treated with PT (Fig 4.10A). The protection offered by the custom peptides against PT-induced cell death was significantly higher (10 to 13%) ($p \leq 0.05$) compared to that of mouse 2.5S-NGF (positive control). Scrambled peptide (100 ng/mL) pre-treatment did not increase the cell viability against PT (4.10A). Moreover, post-treatment of PT-treated cells with TNP or HNP or co-treatment with TNP or HNP with PT did not restore the cell viability against PT-induced toxicity (Figs 4.10B-C).

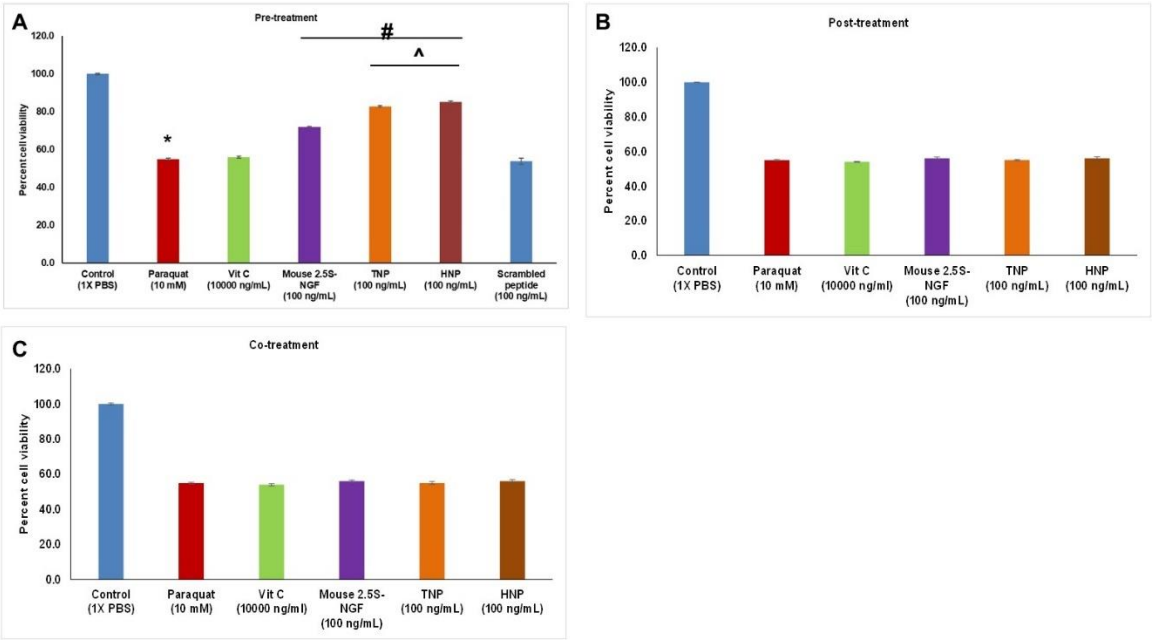

Fig 4.10 Determination of the protective effects of custom peptides against PT-induced cell death. The viability of PC-12 cells was determined by MTT assay. (A) Pre-treatment of cells with custom peptides (100 ng/mL, ~71 nM) or vitamin C (10000 ng/mL) for 4 h followed by PT treatment for 24 h at 37°C in a CO_2 incubator. $^{*}p \leq 0.05$, a significant difference between untreated (control) and PT-treated cells; $^{\#}p \leq 0.05$, a significant difference between PT-treated cells with respect to mouse 2.5S-NGF and custom peptide pre-treated PC-12 cells. $^{\wedge}p \leq 0.05$, a significant difference of mouse 2.5S-NGF treated cells with respect to the peptide (TNP and HNP) treated cells. (B) Treatment of cells with PT for 24 h followed by treatment with custom peptide for 4h. There is no significant

difference in the cell viability in PT-treated cells with respect to mouse 2.5S-NGF, Vit C, and peptide post-treatment. (C) The cells were simultaneously treated with custom peptides and PT for 24 h followed by an assay of cell viability. There is no significant difference in the cell viability in PT-treated cells with respect to mouse 2.5S-NGF, Vit C, and peptide co-treatment. Values are mean ± SD of triplicate determinations.

HNP/TNP at a concentration of 100 ng/mL (~71 nM) for a one-hour pre-incubation showed the optimum protection (up to 80 to 85 % cell viability) against PT-induced (10 mM) cell toxicity (Figs 4.11A-B). The protective potential of the custom peptides was also confirmed by the inhibition of PT-induced release of LDH from PC-12 cells. The maximum release (considered as 100%) of LDH enzyme was observed in control (Triton X-treated) PC-12 cells. Only PT-treated PC-12 cells showed a 50% release of LDH enzyme, compared to only triton-X-100 treated cells. Pre-treatment with the custom peptides (100 ng/mL, ~71 nM) demonstrated a significant decrease (28 to 29%) ($p \leq 0.05$) in the release of the marker enzyme (LDH), compared to that released from PT-treated PC-12 cells (Fig 4.11C). The custom peptides showed a 13 to 14% decrease in the release of LDH enzyme, compared to that of mouse 2.5S-NGF (positive control) (Fig 4.11C). Mouse 2.5S-NGF (100 ng/mL, positive control) was less effective in protecting the PT-induced cell death, according to the results from both the MTT-based cell cytotoxicity assay (Fig 4.11A-B) and the LDH release assay (Fig 4.11C), when comparing the same concentrations of HNP and TNP.

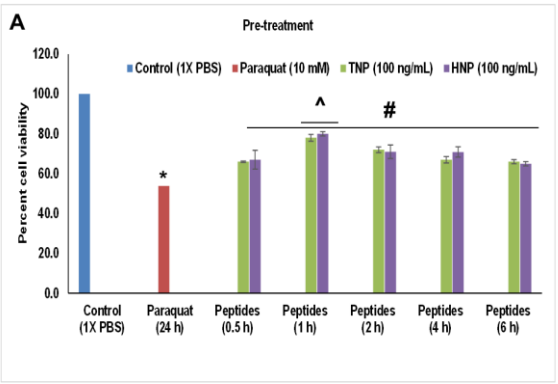

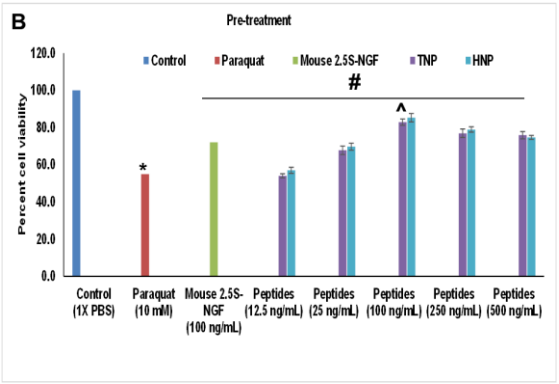

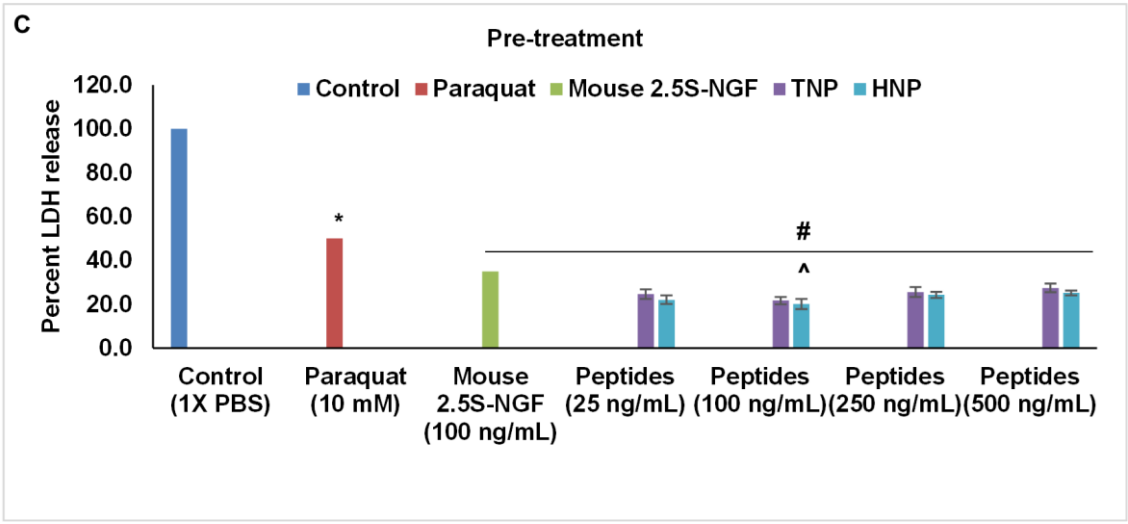

Fig 4.11. Determination of the optimum time and doses of peptide for neuroprotective activity against PT-induced toxicity. Time and dose-dependent neuroprotective activity was determined by MTT and LDH assay in PC-12 cells. (A) Pre-treatment of cells with custom peptides (100 ng/mL, ~ 71 nM) at a different time interval (0.5 h - 6 h) followed by PT treatment for 24 h at 37°C in a CO_2 incubator. $^{*}p \leq 0.05$, a significant difference between untreated (control) and PT-treated cells; $^{\#}p \leq 0.05$, a significant difference of PT-treated cells with respect to custom peptide (TNP and HNP) pre-treated PC-12 cells for different time intervals (0.5 - 6 h). Significance of difference in the percent cell viability of custom peptide pre-treated cells incubated for 1 h with respect to 0.5-6 h, $^{\wedge}p \leq 0.05$. (B) Pre-treatment of cells with different concentrations of custom peptides (12.5 ng/mL to 500 ng/mL) for 1h (optimum time) followed by PT treatment for 24 h at 37°C in a CO_2 incubator (C) LDH release assay to determine the protective effects of custom peptides on the LDH release of PT-induced PC-12 cell cytotoxicity when pre-treated with different concentrations of custom peptides (25 ng/mL to 500 ng/mL) for 1h followed by PT treatment for 24 h at 37°C in a CO_2 incubator. $^{*}p \leq 0.05$, a significant difference between untreated (control) and PT-treated cells; $^{\#}p \leq 0.05$, a significant difference of PT-treated cells with respect to custom peptide (TNP and HNP) pre-treated PC-12 cells for different time intervals (0.5-6 h). Significance of difference in the percent cell viability of custom peptide pre-treated cells at the dose of 100 ng/mL with respect to 12.5-500 ng/mL, $^{\wedge}p \leq 0.05$. Values are mean ± SD of triplicate determinations.

4.1.7 Inhibition of PT-induced ROS production in PC-12 cells

The custom peptides TNP and HNP demonstrated increased antioxidant activity in an increasing concentration-dependent manner up to 100 ng/mL (Fig 4.12A). The custom peptide-mediated reduction in intracellular ROS generation in PC-12 cells was determined by flow cytometry analysis (Figs 4.12B-E). The data shows a significant increase ($p \leq 0.05$) in intracellular ROS production (2.1-fold-change) in PT-treated PC-12 cells compared to control PC-12 cells. Nevertheless, pre-treatment of PC-12 cells with 100 ng/mL (~71 nM) of TNP or HNP significantly diminished (1.6 to 1.8-fold-change) the ROS production (Fig 4.12E). HNP, compared to TNP, showed superior potency (0.23-fold decrease compared to the custom peptide TNP; $p \leq 0.05$) in inhibiting the PT-induced ROS generation (Figs 4.12B-E).

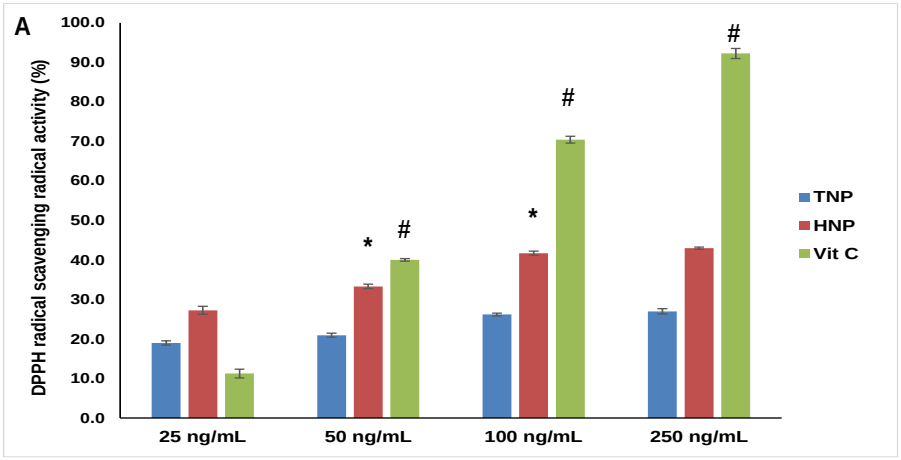

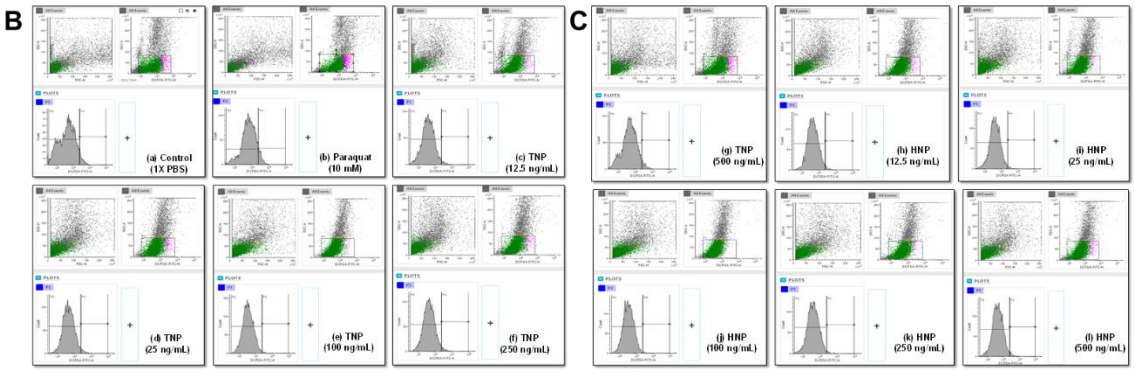

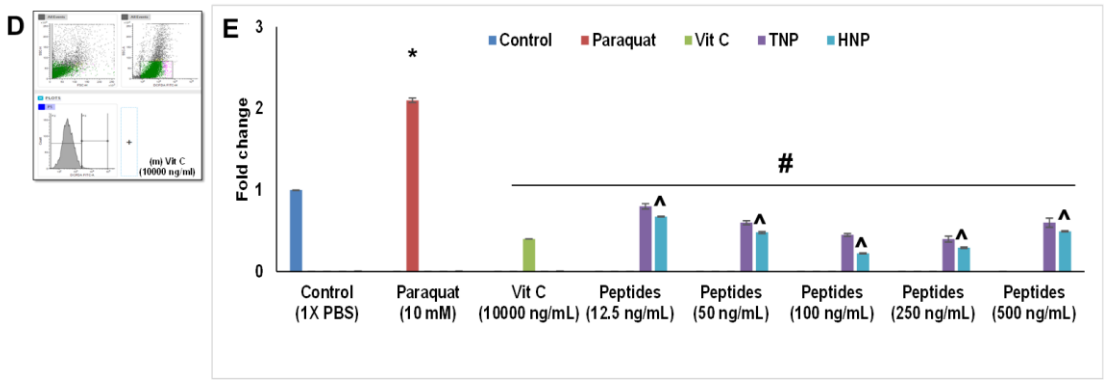

Fig 4.12 Determination of PT-induced intracellular ROS generation and its inhibition by pre-treatment with custom peptide (12.5 ng/mL to 500 ng/mL) and Vitamin C (positive control, 10000 ng/mL) for 1 h followed by the PT treatment for 24 h at 37°C in a CO_2 incubator. The ROS generation was determined by using an H_2DCFDA fluorescence probe and expressed as a fold change value with respect to the control (1x PBS). (A) Determination of *in vitro* concentration-dependent (25-250 ng/mL) DPPH radical-scavenging activity of custom peptides. $^{*}p < 0.05$ significant difference between different concentrations of custom peptide HNP; $^{\#}p < 0.05$ significant difference between the different concentrations of vit C. (B-D) Flow cytometric determination of intracellular ROS. (E) Bar graph representing quantitative analysis of the intracellular ROS generation (expressed by fold change value with respect to control) determined by flow cytometry analysis. $^{*}p \leq 0.05$, a significant difference between untreated (control) and PT-treated cells; $^{\#}p \leq 0.05$, a significant difference of PT-treated cells with respect to custom peptides (TNP and HNP) and vit C pre-treated cells. Significance of difference in the fold change value in between TNP and HNP at the dose of 12.5 to 100 ng/mL, $^{\wedge}p \leq 0.05$. Values are mean ± SD of triplicate determinations.

The spectrofluorometric analysis also validated the custom peptide-mediated reduction in intracellular ROS generation by PT in PC-12 cells. PT treatment (10 mM) resulted in a 2-fold increase in ROS production compared to control PC-12 cells (Fig 4.13). A significant decrease ($p \leq 0.05$) in ROS levels with increasing concentration of peptides was observed in PC-12 cells pre-treated with HNP or TNP (up to 100 ng/mL, equivalent to 71 nM), compared to PT-treated PC-12 cells (Fig 4.13). Nevertheless, above this concentration, the PT-induced ROS production could not be decreased by the peptides (Fig 4.13). The custom peptides at a concentration of 100 ng/mL (~71 nM) demonstrated superior inhibition (0.6 to 0.8-fold decrease) ($p \leq 0.05$) of the PT-induced

ROS generation, compared to that offered by Vitamin C (positive control) (0.3-fold decrease) at a higher concentration (10000 ng/mL).

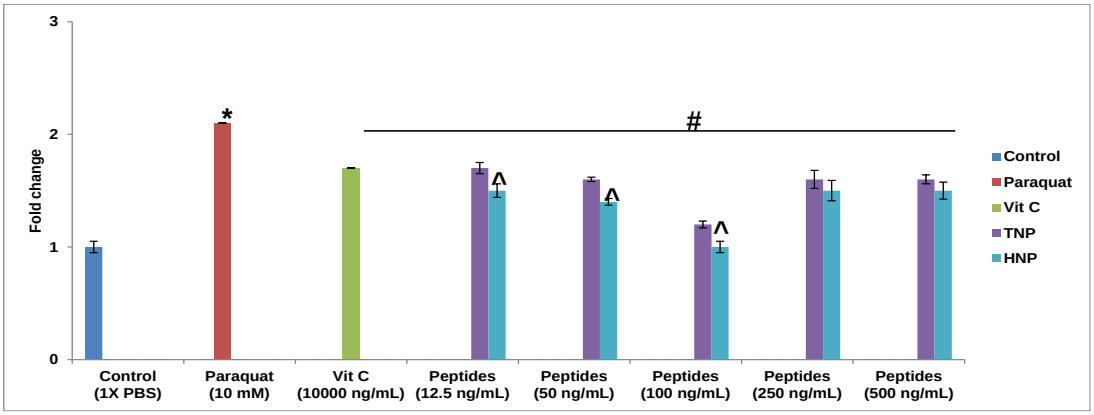

Fig 4.13 Spectrofluorometric determination of intracellular ROS. $^{*}p < 0.05$, a significant difference between untreated (control) and PT-treated cells; $^{\#}p < 0.05$, a significant difference of PT-treated cells with respect to custom peptides (TNP and HNP) and Vit C pre-treated cells. Significance of difference in the fold change value between TNP and HNP at the dose of 12.5 to 100 ng/mL, $^{\wedge}p < 0.05$. Values are mean ± SD of triplicate determinations.

4.1.8 Inhibition of PT-induced depolarization of mitochondrial membrane in PC-12 cells

JC-1 staining was used to study whether or not the custom peptides could restore the loss of mitochondrial membrane potential (MMP) triggered by PT in PC-12 cells. JC-1 signals red fluorescence in non-apoptotic cells as it forms an aggregate when it penetrates non-apoptotic cells, but it signals green fluorescence as the monomeric form in apoptotic cells. The red/green fluorescence ratio was quantified from confocal images to show the change in MMP (Figs 4.14A-B). The fluorescence intensity of the red/green ratio was significantly reduced ($p \leq 0.05$) by 90% in PT-treated cells, compared to control (1XPBS) PC-12 cells (Fig 4.14B). The fluorescence intensity of the red/green ratio was significantly restored ($p \leq 0.05$) by 60 to 65% when PC-12 cells were pre-treated for 1 h with the TNP or HNP custom peptides and then followed by PT-treatment (Figs 4.14A-B). This data suggests that pre-treatment with TNP/ HNP increases cell resistance against PT-induced mitochondrial membrane depolarization. Moreover, HNP showed a

significantly higher (0.4-fold increase) inhibition ($p \leq 0.05$) of MMP, when compared to TNP.

MMP was also quantified by flow cytometry analysis using JC-1 staining. Red fluorescence is high when MMP is high, and green fluorescence is high when MMP is low. The PT-treated (10 mM) PC-12 cells showed an increase of 50% in green fluorescence, compared to the untreated PC-12 cells, indicating a disrupted MMP. Custom peptide pre-treatment (100 ng/mL, ~71 nM) resulted in a significant 40 to 45% increase ($p \leq 0.05$) in the intensity of red fluorescence when compared to the PC-12 cells that were only PT-treated (Figs 4.14C-D). The data showed a significant increase ($p \leq 0.05$) in mitochondrial membrane depolarisation in the PT-treated PC-12 cells (a 2-fold decrease in red/green fluorescence) compared to the control PC-12 cells. Nevertheless, pre-treating PC-12 cells with TNP or HNP restored (1.3-1.7-fold increase in the red/green fluorescence) the PT-induced mitochondrial membrane depolarization, and HNP showed a significantly ($p \leq 0.05$) higher (0.4-fold) activity compared to TNP (Figs 4.14C-D).

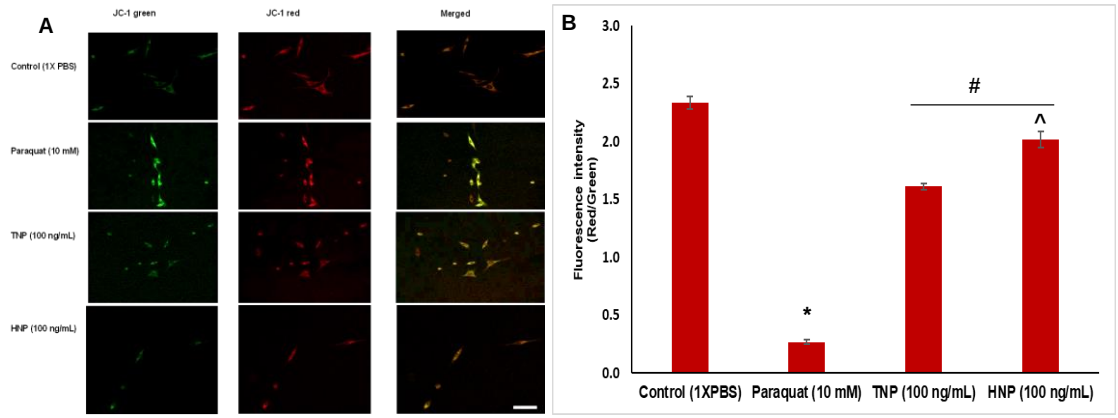

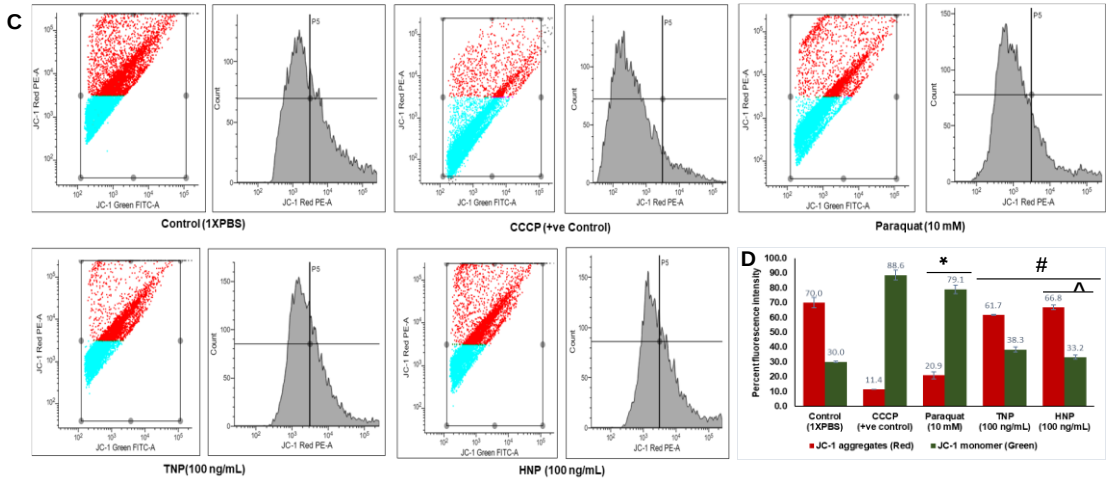

Fig 4.14 Restoration of PT-induced disruption of mitochondrial membrane potential (MMP) of PC-12 cells pre-treated with custom peptides (100 ng/mL, ~71 nM) for 1 h followed by the PT treatment for 24 h at 37°C in a CO_2 incubator. The PT-treated (10 mM) PC-12 cells pre-treated with or without custom peptide (~71 nM) were observed for the measurement of the ratio of red/green fluorescence intensity by JC-1 staining. (A) Confocal images of PC-12 cells stained with JC-1 dye to measure the MMP micrographed at the magnification of 40X. JC-1 red fluorescence represents normal MMP, whereas JC-1 green fluorescence indicates damaged MMP. The scale bar indicates the length as 20 µm. (B) Bar diagram representing the ratio of red/green fluorescence intensity quantified using Image J software. (C) The fluorescence signal intensity of JC-1 monomer and JC-1 aggregates was determined by flow cytometry analysis. Carbonyl cyanide m-chlorophenyl hydrazone (CCCP) is a mitochondrial uncoupling agent that depolarises the mitochondria taken as a positive control. (D) Bar graph representing quantitate analysis of the red and green fluorescence intensity detected by the flow cytometry. $^{*}p \leq 0.05$, a significant difference between untreated (control) and PT-treated cells; $^{\#}p \leq 0.05$, a significant difference of PT-treated cells with respect to custom peptides (TNP and HNP) pre-treated cells. Significance of difference in fluorescence intensity between TNP and HNP, $^{\wedge}p \leq 0.05$. Values are mean ± SD of triplicate determinations.

4.1.9 Restoration of PT-induced cellular and nuclear morphological changes and apoptotic cells by the custom peptide pre-treated PC-12 cells

The anti-apoptotic potential of custom peptides (100 ng/mL, ~71 nM) against PT-induced (10 mM) apoptotic cell death was determined by flow cytometry analysis (Figs 4.15A-

B). PT (10 mM) induced a significant increase ($p \leq 0.05$) (10-11%) in apoptotic cell death, compared to untreated (control) PC-12 cells (Figs 4.15A-B). HNP and TNP; however, at a concentration of 100 ng/mL (~71 nM) significantly inhibited ($p \leq 0.05$) apoptotic and necrotic cell death (by 5-7%) induced by PT, when compared to PC-12 cells that had only been PT-treated (Figs 4.15A-B), and like previous analyses, HNP showed 3.3%increase in activity than TNP.

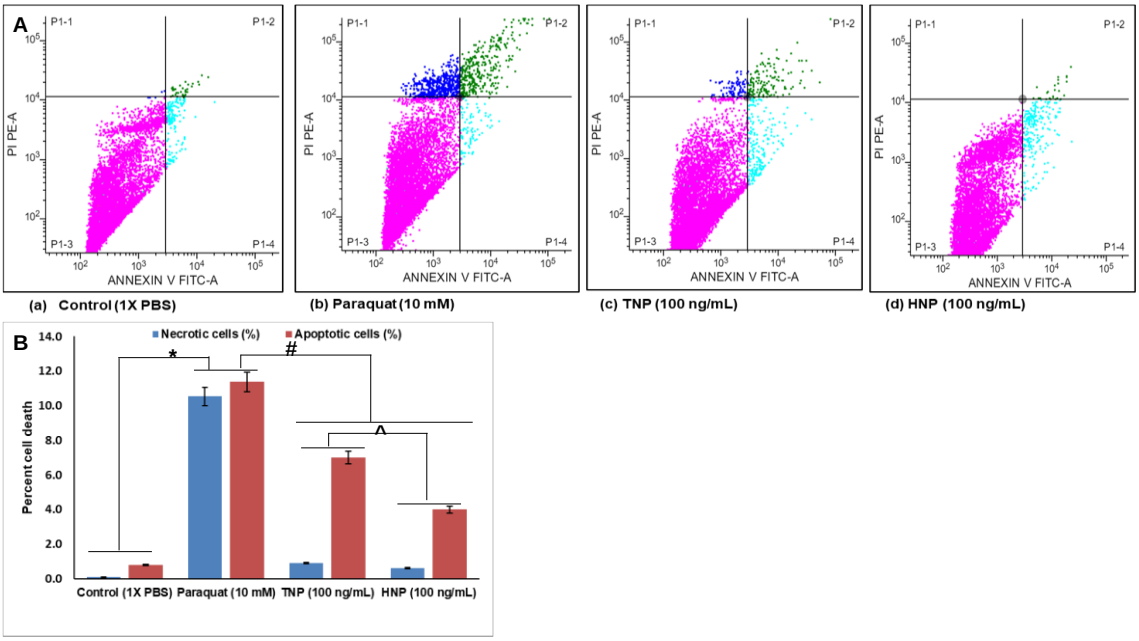

Fig 4.15 Effects of the custom peptide (100 ng/mL) on inhibition of PT-induced apoptosis in PC-12 cells pre-treated with custom peptides (100 ng/mL, ~71 nM) for 1 h followed by the PT treatment for 24 h at 37°C in a CO_2 incubator. (A) The fluorescence intensity of Annexin V-FITC and Propidium iodide (PI) was determined by flow cytometry. (B) The bar graph represents a quantitative analysis of the percent cell death determined by flow cytometry analysis. $^{*}p \leq 0.05$, a significant difference between untreated (control) and PT-treated cells; $^{\#}p \leq 0.05$, a significant difference of PT-treated cells with respect to custom peptides (TNP and HNP) pre-treated cells. Significance of difference in percent cell death between TNP and HNP, $^{\wedge}p \leq 0.05$. Values are mean ± SD of triplicate determinations.

Confocal image analysis revealed a decrease in the population of PT-treated PC-12 cells, compared to untreated (control) PC-12 cells (Fig 4.16A). Induction of cell death by PT in the PC-12 cells was evident from the cell morphology (DAPI staining), shrunken

nuclei, membrane blebbing, and secondary cellular necrosis (Fig 4.16A). The percent of cell death characterized by cellular and nuclear morphological changes increased by 21% when cells were treated with PT, but the pre-treatment with custom peptides significantly reduced ($p \leq 0.05$) the degree of cell death (4.6 - 7.9%). HNP showed a higher activity compared to TNP (Fig 4.16B).

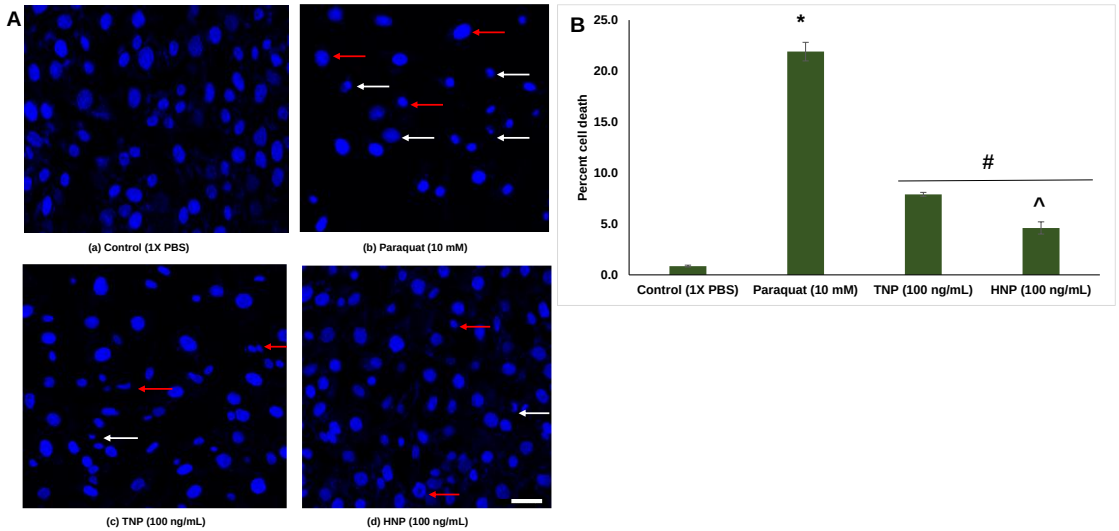

Fig 4.16 Effects of the custom peptide (100 ng/mL) on inhibition of PT-induced apoptosis in PC-12 cells pre-treated with custom peptides (100 ng/mL, ~71 nM) for 1 h followed by the PT treatment for 24 h at 37°C in a CO2 incubator. (A) Confocal microscopic analysis of changes in the cellular and nuclear morphology of PC-12 cells by DAPI staining at the magnification of 40X. The red arrows indicate cells with membrane blebbing and shrunken nuclei, and the white (solid) arrows indicate secondary cellular necrosis. The scale bar indicates the length of 20 µm. (B) The bar diagram shows the percent cell death determined from the changes in the cellular and nuclear morphology with respect to the control (1x PBS). The intensity of the DAPI staining was determined using Image J software. $^{*}p < 0.05$, a significant difference between untreated (control) and PT-treated cells; $^{\#}p < 0.05$, a significant difference of PT-treated cells with respect to custom peptides (TNP and HNP) pre-treated cells. Significance of difference in percent cell death between TNP and HNP, $^{\wedge}p < 0.05$. Values are mean ± SD of triplicate determinations.

4.1.10 Custom peptide pre-treatment restored the paraquat-induced upregulated and downregulated pro- and anti-apoptotic genes to delay paraquat-induced programmed cell death in PC-12 cells

The qRT-PCR analysis demonstrated a 1.5 to 2-fold-change increase ($p \leq 0.05$) in the expression of proapoptotic genes (cyt-C, bax, bid), and a 3.4 to 3.5-fold change increase in the expression of heat shock gene-70 (hsp-70), and caspase-3 gene (a hallmark of apoptosis) in the PT group compared to the CT group of cells (Fig 4.17). The pre-treatment of cells with mouse 2.5S-NGF (positive control) and TNP or HNP resulted in a significant downregulation ($p \leq 0.05$) or restoration of the expression of the genes that had been upregulated by PT treatment alone (Fig 4.17). The qRT-PCR analyses showed a 0.3-fold decrease in the expression of anti-apoptotic genes (bcl-2) in the PT group compared to the CT group of cells. Further, pre-treatment with TNP or HNP, and mouse 2.5S-NGF (positive control) restored the downregulated anti-apoptotic (bcl-2) genes in the PT group of cells (Fig 4.17).

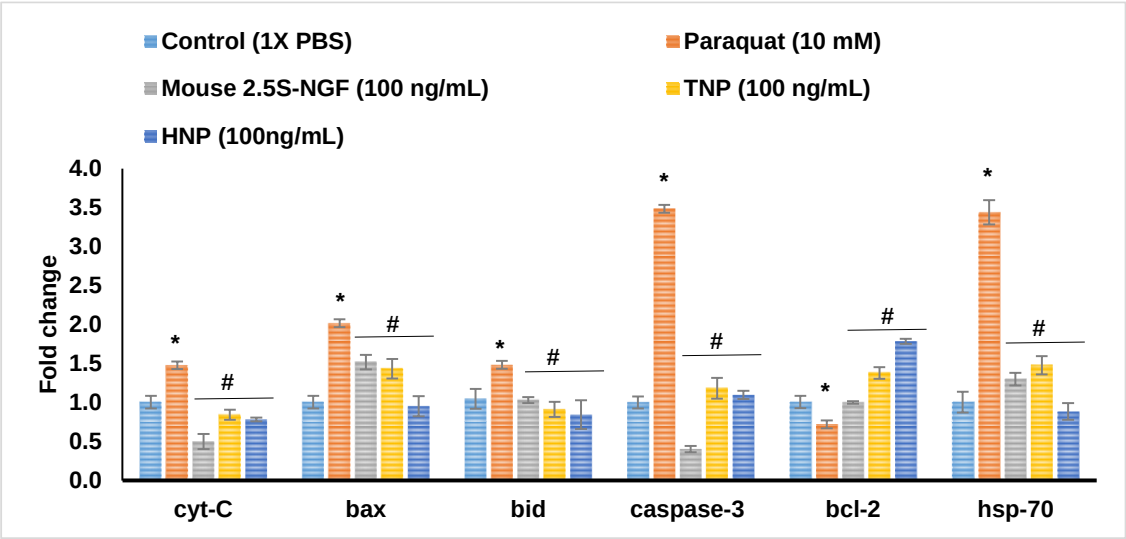

Fig 4.17 The qRT-PCR analysis to show the expression of key pro-/anti-apoptotic genes in PC-12 cells post-treatment with paraquat (10 mM) for 12 h, and comparison with the custom peptides (100 ng/mL, ~71 nM) /mouse 2.5S-NGF (positive control, 100 ng/mL) pre-treatment for 1 h followed by the PT treatment for 12 h at 37°C in a CO_2 incubator. The expression of mRNA was normalized using the housekeeping gene GAPDH. $^{*}p \leq 0.05$, a significant difference between untreated (control) and PT-treated cells; $^{\#}p \leq 0.05$, a significant difference of PT-treated cells with respect to custom peptides (TNP and

HNP)/mouse 2.5S-NGF pre-treated cells. Values are mean ± SD of triplicate determinations.

4.1.11 Comparing the differential expression of cellular proteins in the PT-treated PC-12 cells and the cells pre-treated with custom peptides by quantitative mass spectrometry

LC-MS/MS analysis unambiguously identified 207 non-redundant proteins from the four groups of PC-12 cells (PT, PHNP, CT, and HNP). Based on their intracellular locations and biological processes, the proteins were classified into nine distinct categories, among which three major cellular proteins were present in high relative abundances compared to the other proteins (Table 4.4).

Table 4.4 The quantitative proteomics data shows the relative abundance of the intracellular proteins in the different treatment groups. The relative abundance of the proteins was calculated by the MS2-based spectral count method. For comparison of differential expression of the cellular proteins, the PC-12 cells were subjected to the following treatments at 37°C: (a) 1X PBS (control) treated PC-12 cells (CT), (b) 10 mM paraquat (PT) treatment for 24 h, (c) pre-treatment with 100 ng/mL (~71 nM) custom peptide for 1 h followed by 10 mM paraquat treatment (PHNP) for 24 h, and (d) treatment with 100 ng/mL (~71 nM) of custom peptide (HNP) for 1 h.

Accession No	**Relative abundance of 1X PBS (control) treated PC-12 cells (CT)**	**Relative abundance of PC-12 cells pre-treated with 100 ng/mL (~71 nM) custom peptide for 1 h followed by 10 mM paraquat treatment (PHNP) for 24 h**	**Relative abundance of PC-12 cells treated with 10 mM paraquat (PT) for 24 h**	**Relative abundance of PC-12 cells treated with 100 ng/mL (~71 nM) of custom peptide (HNP) for 1 h**
Antioxidant/Stress response				
P06761|BIP_RAT	0.51	0.93	3.08	0.63
P63018|HSP7C_RAT	0.51	0.80	2.51	0.62
Q07936|ANXA2_RAT	0.51	0.62	2.51	0.58
Q66HD0|ENPL_RAT	0.51	0.97	2.76	0.67
P34058|HS90B_RAT	0.51	1.02	2.51	0.60
P48679|LMNA_RAT	0.51	0.88	2.92	0.60
Q00715|H2B1_RAT	0.51	0.75	4.18	0.72
Q9Z0V5|PRDX4_RAT	0.51	0.99	2.51	0.67
Binding protein				
tr|G3V6P7|G3V6P7_RAT	0.68	0.79	2.51	0.72
P68035|ACTC_RAT	0.51	0.88	2.76	0.73

tr|Q5RJR9|Q5RJR9_RAT	0.51	0.68	2.51	0.49
P13832|MRLCA_RAT	0.51	0.87	3.34	0.67
P62804|H4_RAT	0.51	0.85	3.01	0.53
P00507|AATM_RAT	0.51	0.99	2.51	0.49
Apoptotic protein				
P63039|CH60_RAT	0.51	0.92	2.51	0.63
P62630|EF1A1_RAT	0.51	0.62	2.51	0.80
P11240|COX5A_RAT	0.51	0.99	2.51	0.49
P62898| Cycs_RAT	0.51	0.99	2.51	0.50
P00787|CATB_RAT	0.51	0.99	2.51	0.48
Mitochondrial protein				
P10860|DHE3_RAT	0.51	0.90	2.51	0.49
P04636|MDHM_RAT	0.51	0.83	2.51	0.49
P32551|QCR2_RAT	0.51	0.99	2.51	0.49
P00507|AATM_RAT	0.51	0.99	2.51	0.49
ATP synthesis				
P10719|ATPB_RAT	0.51	2.73	0.90	3.61
P15999|ATPA_RAT	0.51	2.92	0.91	3.63
Neuronal development				
Q9JLT0|MYH10_RAT	0.51	2.51	0.69	3.57
P18418|CALR_RAT	0.51	2.51	0.79	3.69
P31000|VIME_RAT	0.51	3.01	0.93	
Innate immune response				

P07150|ANXA1_RAT	0.51	0.75	2.51	0.69
P11598|PDIA3_RAT	0.51	0.81	2.51	0.49
Structural protein				
Q64119|MYL6_RAT	0.51	0.76	2.51	0.63
Endoplasmic reticulum protein				
tr|D3ZH41|D3ZH41_RAT	0.51	0.80	2.51	0.49

The quantitative analysis showed differential expression of proteins in the PT group of PC-12 cells versus the CT group. A total of 130 intracellular proteins were identified in the PT group (Fig 4.18A), of which 118 proteins were differentially regulated compared to those in the CT group (Fig 4.18A). Among the 118 identified proteins, the PT-induced altered expression of 27 proteins was restored in PC-12 cells that had been pre-treated with HNP (Fig 4.18A). Notably, six intracellular proteins were regulated differently in the PHNP and PT groups (Fig 4.18A). Two proteins (keratin type 1 and type 2 cytoskeletal proteins) were uniquely expressed in the PHNP group.

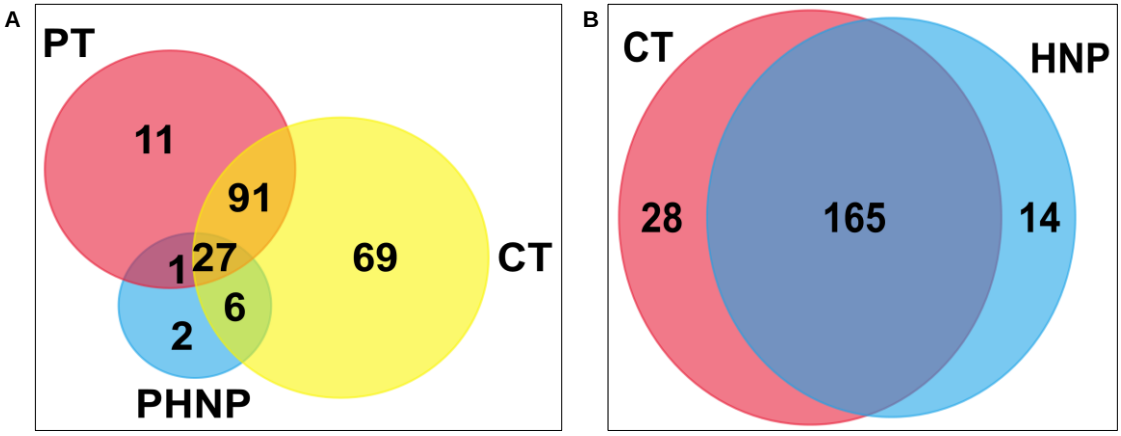

Fig 4.18 (A) Venn diagram showing the common intracellular proteins among untreated (control) (CT), PT (PT) treated, and HNP pre-treated followed by PT-treated (PHNP) groups of PC-12 cells determined by LC/MS-MS analysis. (B) Venn diagram showing common intracellular proteins among untreated (control) (CT) and only HNP-treated PC-12 cells determined by LC/MS-MS analysis.

Intracellular proteins in the PHNP group were also compared in the PT and CT groups to identify differentially expressed proteins involved in apoptosis (60 kDa heat shock protein (hsp-60), cytochrome C (cycs), Heat shock cognate 71 kDa (hspa8), the electron transport chain (cytochrome c oxidase subunit 5A; cox5a), cytochrome b-c1 complex subunit 2 (uqcrc2) stress response (heat shock protein (hsp 90-beta), antioxidant function (peroxiredoxin-4 (prdx-4), glutamate dehydrogenase 1 (glud-1), Wnt signaling (actin, (actc1), signal transduction (cytoskeleton-associated protein 4, (ckap4), the innate immune response annexin A2 (anaxa2), collagen biosynthesis (collagen-binding protein (serpinh1), and phagocytosis (cathepsin B (ctsb). PT treatment of the PC-12 cells caused the upregulation of some proteins involved in these pathways (Table 4.5A), and their

expression was restored in the PHNP treatment group. Their fold-change values are mentioned in Table 4.5A. In contrast, some proteins involved in neuronal development and ATP synthesis pathways were downregulated (Table 4.5B), though their expression was restored in the PHNP group (Table 4.5B).

Table 4.5 Comparison of the fold changes in differential expression of proteins in PT-treated PC-12 cells determined by proteomic analysis.

(A) List of up-regulated proteins in PT-treated PC-12 cells compared to untreated (control) PC-12 cells, and their downregulation in cells pre-treated with HNP.				
Accession	**PT treatment (fold change compared to control)**	**HNP pre-treatment, (fold change compared to control)**	**Pathway name**	**Description**
P06761|BIP_RAT	6.00	1.81	Apoptosis signaling pathway	Endoplasmic reticulum chaperone BiP OS=Rattus norvegicus OX=10116 GN=Hspa5 PE=1 SV=1
P63018|HSP7C_RAT	4.87	1.56	Apoptosis signaling pathway	Heat shock cognate 71 kDa protein OS=Rattus norvegicus OX=10116 GN=Hspa8 PE=1 SV=1
Q07936|ANXA2_RAT	4.87	1.21	Antioxidant pathway	Annexin A2 OS=Rattus norvegicus OX=10116 GN=Anxa2 PE=1 SV=2
Q66HD0|ENPL_RAT	5.36	1.88	Stress response pathway	Endoplasmin OS=Rattus norvegicus OX=10116 GN=Hsp90b1 PE=1 SV=2
P34058|HS90B_RAT	4.87	1.99	Stress response pathway	Heat shock protein HSP 90-beta OS=Rattus norvegicus OX=10116 GN=Hsp90ab1 PE=1 SV=4
P48679|LMNA_RAT	5.68	1.71	Apoptosis signaling pathway	Prelamin-A/C OS=Rattus norvegicus OX=10116 GN=Lmna PE=1 SV=1
Q00715|H2B1_RAT	8.12	1.46	Stress response pathway	Histone H2B type 1 OS=Rattus norvegicus OX=10116 PE=1 SV=2

Q9Z0V5|PRDX4_RAT	4.87	1.93	Stress response pathway	Peroxiredoxin-4 OS=Rattus norvegicus OX=10116 GN=Prdx4 PE=2 SV=1
tr|G3V6P7|G3V6P7_RAT	3.69	1.16	Phagocytosis	Myosin, heavy polypeptide 9, non-muscle OS=Rattus norvegicus OX=10116 GN=Myh9 PE=1 SV=1
P68035|ACTC_RAT	5.36	1.81	Wnt signalling pathway	Actin, alpha cardiac muscle 1 OS=Rattus norvegicus OX=10116 GN=Actc1 PE=2 SV=1
tr|Q5RJR9|Q5RJR9_RAT	4.87	1.71	Collagen biosynthesis	Collagen-binding protein OS=Rattus norvegicus OX=10116 GN=Serpinh1 PE=1 SV=1
P13832|MRLCA_RAT	6.50	1.33	Cell cycle	Myosin regulatory light chain RLC-A OS=Rattus norvegicus OX=10116 GN=Rlc-a PE=2 SV=2
P62804|H4_RAT	5.85	1.69	Transcription regulation	Histone H4 OS=Rattus norvegicus OX=10116 GN=H4c2 PE=1 SV=2
P00507|AATM_RAT	4.87	1.65	Asparagine and aspartate biosynthesis	Aspartate aminotransferase, mitochondrial OS=Rattus norvegicus OX=10116 GN=Got2 PE=1 SV=2
P63039|CH60_RAT	4.87	1.78	Apoptosis signaling pathway	60 kDa heat shock protein, mitochondrial OS=Rattus norvegicus OX=10116 GN=Hspd1 PE=1 SV=1

P62630|EF1A1_RAT	4.87	1.21	Protein biosynthesis	Elongation factor 1-alpha 1 OS=Rattus norvegicus OX=10116 GN=Eef1a1 PE=2 SV=1
P11240|COX5A_RAT	4.87	1.93	Electron transport chain	Cytochrome c oxidase subunit 5A, mitochondrial OS=Rattus norvegicus OX=10116 GN=Cox5a PE=1 SV=1
P62898| Cycs_RAT	4.87	1.93	Apoptosis signaling pathway	Cytochrome c OS=Rattus norvegicus OX=10116 GN= Cycs PE=3 SV=1
P00787|CATB_RAT	4.87	1.93	Phagocytosis	Cathepsin B OS=Rattus norvegicus OX=10116 GN=Ctsb PE=1 SV=2
P10860|DHE3_RAT	4.87	1.75	Antioxidant	Glutamate dehydrogenase 1, mitochondrial OS=Rattus norvegicus OX=10116 GN=Glud1 PE=1 SV=2
P04636|MDHM_RAT	4.87	1.61	Pyruvate metabolism	Malate dehydrogenase, mitochondrial OS=Rattus norvegicus OX=10116 GN=Mdh2 PE=1 SV=2
P32551|QCR2_RAT	4.87	1.93	Electron transport chain	Cytochrome b-c1 complex subunit 2, mitochondrial OS=Rattus norvegicus OX=10116 GN=Uqcrc2 PE=1 SV=2
P07150|ANXA1_RAT	4.87	1.45	Innate immune response	Annexin A1 OS=Rattus norvegicus OX=10116 GN=Anxa1 PE=1 SV=2
P11598|PDIA3_RAT	4.87	1.58	Vitamin D metabolism	Protein disulfide-isomerase A3 OS=Rattus norvegicus OX=10116 GN=Pdia3 PE=1 SV=2

Q64119|MYL6_RAT	4.87	1.48	Motor function	Myosin light polypeptide 6 OS=Rattus norvegicus OX=10116 GN=Myl6 PE=1 SV=3
tr|D3ZH41|D3ZH41_RAT	4.87	1.55	Signal transduction	Cytoskeleton-associated protein 4 OS=Rattus norvegicus OX=10116 GN=Ckap4 PE=1 SV=2
(B) List of down-regulated proteins in PT treated PC-12 cells compared to untreated (control) PC-12 cells and their upregulation in cells pre-treated with HNP.				
Accession	**Paraquat treatment (fold change with respect to control)**	**HG17 pre-treatment, (fold change with respect to control)**	**Pathway name**	**Description**
P10719|ATPB_RAT	1.76	3.02	ATP synthesis	ATP synthase subunit beta, mitochondrial OS=Rattus norvegicus OX=10116 GN=Atp5f1b PE=1 SV=2
P15999|ATPA_RAT	1.77	3.22	ATP synthesis	ATP synthase subunit alpha, mitochondrial OS=Rattus norvegicus OX=10116 GN=Atp5f1a PE=1 SV=2
Q9JLT0|MYH10_RAT	1.34	3.63	Neuronal development	Myosin-10 OS=Rattus norvegicus OX=10116 GN=Myh10 PE=1 SV=1
P18418|CALR_RAT	1.54	3.17	Neuronal development	Calreticulin OS=Rattus norvegicus OX=10116 GN=Calr PE=1 SV=1
P31000|VIME_RAT	1.05	5.85	Neuronal development	Vimentin OS=Rattus norvegicus OX=10116 GN=Vim PE=1 SV=2
O08878|GPER1_RAT	1.20	3.40	Neuritogenesis	G-protein coupled estrogen receptor 1 OS=Rattus norvegicus OX=10116 GN= Gper1 (Cmkrl2, Gper, Gpr30, Gpr41) SV=2

When comparing the expression of intracellular proteins in the HNP to the CT group of cells, 14 proteins were found to be uniquely expressed in the former group (Fig 4.18B). Therefore, the proteomic analyses provide evidence of uniquely expressed proteins and their associated metabolic pathways in PC-12 cells treated with HNP, in comparison to untreated cells (Table 4.6).

Table 4.6 List of the uniquely expressed metabolic pathways in PC-12 cells treated with HNP when compared to untreated PC-12 cells. These pathways are determined by quantitative proteomic analyses.

Mapped IDs	**Pathway name**	**Protein**
RAT|RGD=71000|UniProtKB=Q9JLT0, RAT|RGD=1565476|UniProtKB=Q6P9V9	Cytoskeletal regulation by Rho GTPase	Tuba1b, Plec
RAT|RGD=2451|UniProtKB=P62898, RAT|RGD=621379|UniProtKB=Q06647, RAT|RGD=68374|UniProtKB=P10888	ATP synthesis	Cycs, Cox4i1, Atp5
RAT|RGD=71000|UniProtKB=Q9JLT0	Nicotinic acetylcholine receptor signalling pathway	Myh10
RAT|RGD=71000|UniProtKB=Q9JLT0	Inflammation mediated by chemokine and cytokine signaling pathway	Myh10
RAT|RGD=1565476|UniProtKB=Q6P9V9	Gonadotropin-releasing hormone receptor pathway	Tuba1b
RAT|RGD=71006|UniProtKB=Q63692, RAT|RGD=1305960|UniProtKB=Q498E0	Stress response antioxidant pathway	Txndc12, Plec

The PPI network revealed the functional significance of the intracellular proteins and their involvement in particular pathways (Fig 4.19). The cellular pathways governed by the 27 differentially regulated proteins in the CT, PT, and PHNP groups of PC-12 cells were curated manually and the interaction network was established to highlight the interconnected pathways (Fig 4.19).

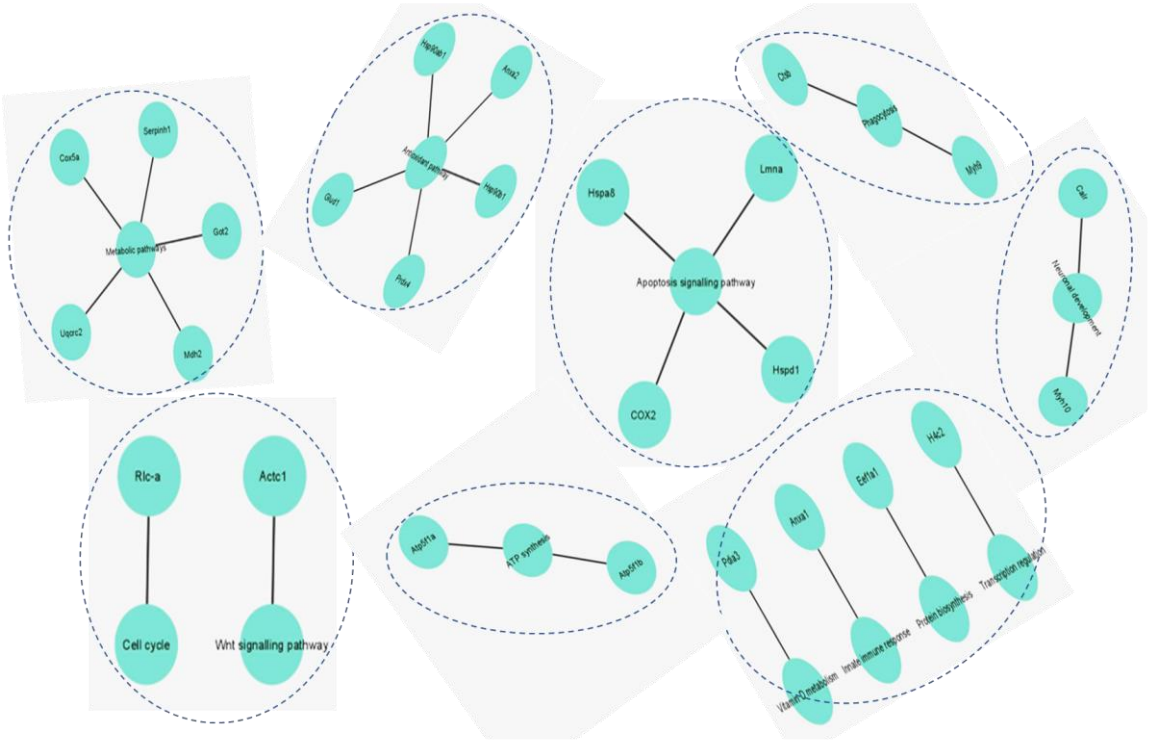

Fig 4.19 Molecular network of HNP-mediated neuroprotection drawn in Cytoscape (version 3.9.1). The molecular network shows the multiple pathways that are interconnected to each other and involved in the HNP-mediated neuroprotection. The proteins involved in the pathways were determined by LC/MS-MS analysis.

Based on the information on the neuritogenesis potency of the custom peptides, inhibition of downstream signaling pathways by specific inhibitors (MAPK-ERK, PI3K/AKT pathways), the neuroprotective potential of custom peptides (via different mechanisms such as inhibition of ROS generation, restoration of MMP, anti-apoptotic/necrotic potential), and the differential expression of proteins (determined by quantitative mass spectrometry analysis) involved in neuroprotective activities, the mechanism of action of HNP against PT-induced neuroprotective activity is shown in Fig 4.20.

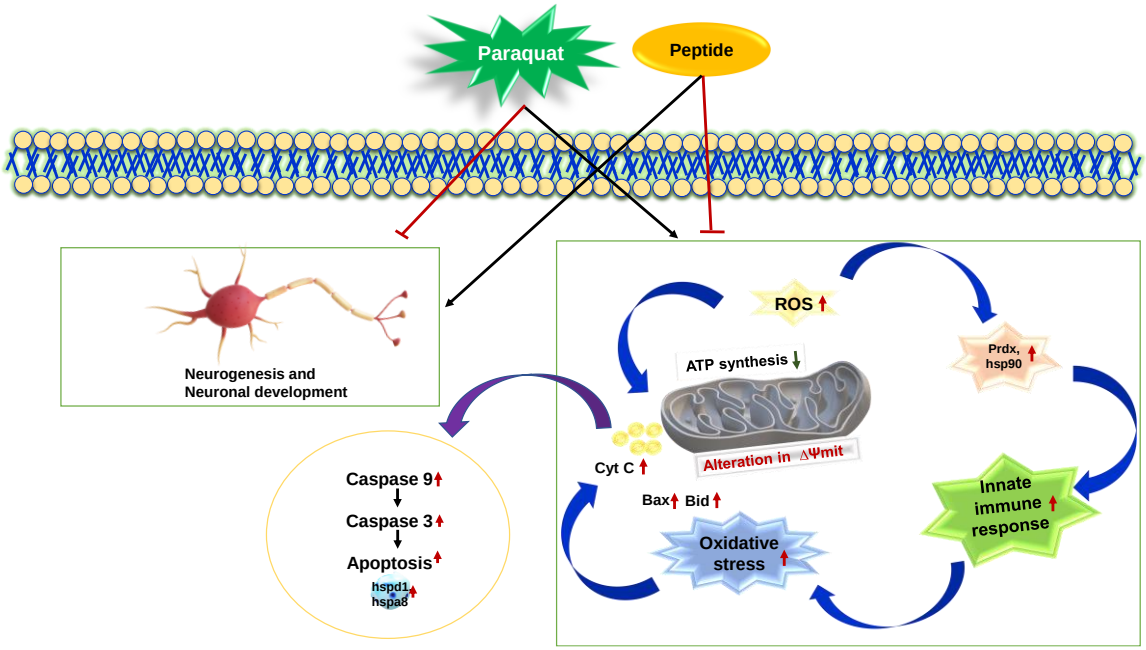

Fig 4.20 The proposed neuroprotection mechanism of custom peptides against PT-induced neurotoxicity in PC-12 cells.

4.2 Discussion

Neuronal differentiation is a vital physiological phenomenon, often associated with intellectual development in children and age-related neurodegenerative diseases such as PD, AD, and Huntington's disease (HD) [4]. Proposing a large neurotrophin polypeptide or a protein molecule as a drug candidate has several disadvantages including its undesired pleiotropic effect, short half-life, proteolytic degradation, and poor pharmacokinetics [5-8]. Therefore, in recent years, the development of small, peptide-based drugs has gained momentum and opened new avenues of research to overcome the limitations of parent molecules [9]. In any case, the peptide-based drugs must show improved neuroprotective effects, synaptic and neuronal plasticity, neuritogenesis, better pharmacokinetics than their larger, parent neurotrophin molecules, and easy penetration to cells via the BBB [8-11].

In this study, two small, water-soluble custom peptides (TNP and HNP, with masses of 1.2 kDa and 1.4 kDa, respectively) and one scrambled peptide (mass of 1.3 kDa) were designed from snake venom neurotrophin molecules to be developed as possible neuroprotective drug prototypes with improved neuritogenesis potency,

compared to mouse 2.5S-NGF (positive control) for the restoration of neurons that have been degenerated by toxic chemicals.

Several studies have demonstrated that computational analysis (docking) is a powerful tool for identifying novel compounds of therapeutic interest with high probability and which can forecast ligand-target interactions at the molecular level with high efficiency [1-3,12-14]. The computational study can assist in screening many compounds (ligands) against specific targets (i.e., a receptor) to identify compounds that can bind efficiently with the target, though *in silico* findings must be confirmed by *in vitro* and *in vivo* studies [1-3,12-14]. The *in silico* analysis demonstrated that domain-3 of the TrkA receptor extracellular domain is the only region that binds with NGF and forms the NGF/TrkA domain-3 complex. Subsequently, the complex induces TrkA dimerization and transduces a signal to activate MAPK and the PI3K/Akt signaling pathways [15]. The docking analysis also demonstrated that, like human NGF molecules, the TNP and HNP custom peptides show high-affinity binding only with domain-3 of the human TrkA receptor; however, the scrambled peptide does not show binding affinity with domain-3 of the human TrkA receptor. The binding site for the custom peptides was also shown to differ from that of the human NGF-TrkA binding site. Therefore, the HNP and TNP peptides are specific for binding to TrkA and CAM-1 receptors.

Since TrkA dimerization is important for activation of the signal transduction mechanism, dimerization of the TrkA receptors after binding to custom peptides needs to be explored. The docking scores of the docked complex (custom peptide and TrkA domain-3) indicate higher binding affinities of TNP towards the TrkA domain-3, compared to that of HNP. Since binding affinity does not always correlate with the stability of the binding, the stability of binding should also be evaluated by a molecular dynamic simulation study and computational analyses. In this study, our findings predicted that HNP (compared to TNP) would form a more stable complex with the TrkA receptor. Differences in the binding affinities and stability of the custom peptides and TrkA receptors can be attributed to the electrostatic interactions (hydrogen bonds) between the charged molecules of the HNP / TrkA domain-3 complex [1-3].

Since the custom peptides were designed to mimic the TrkA binding region of the snake venom neurotrophin molecule, the *in silico* analysis convincingly showed that the

high-affinity binding of HNP or TNP to the TrkA receptor is primarily essential for inducing neuritogenesis. The spectrofluorometric binding assay showed high-affinity binding (low K_d value in picomolar range) to the TrkA receptor expressed in mammalian cell lines (PC-12, MDA-MB-231, MCF7) but not in L6 cells, which lack TrkA receptors, which was further validated by fluorescence microscopic study. In the presence of a chemical inhibitor of the TrkA receptor (K252a), no binding was observed under a fluorescence microscope, confirming that the custom peptides bind with the TrkA receptor exclusively. These *in vitro* binding studies also validated the results of the *in silico* analysis. Further, studies have shown the Kd value of binding of mammalian NGF to TrKA receptor is also $1X10^{-11}$M [16,17], indicating HNP and TNP are of equivalent potency with binding to the same receptor.

Because the *in silico* and *in vitro* binding of ligands to receptors does not necessarily assure their desired therapeutic effect, we also evaluated the neuritogenesis potency of these peptides in PC-12 cells, which is considered to be an appropriate *in vitro* model for neuronal differentiation, development, and neurological diseases [1-3,18,19]. PC-12 cell lines have advantages in being derived from neural crest cells with similar structures and functions, and they are easy to grow and maintain [18]. The induction of neuritogenesis is generally initiated after 4-6 h of incubation with NGF [20]; however; optimum neurite length and differentiation of PC-12 cells observed after 14 days of incubation with snake venom NGFs [1,2] TNP and HNP in this study showed the same result.

In evaluating the neuronal outgrowth-inducing properties of the custom peptides in PC-12 neuronal cells, we found that, as predicted, both peptides significantly increased the neurite length and percent differentiation of PC-12 cells measured simultaneously point, in comparison to the effect of mouse 2.5S-NGF treatment alone. No significant difference was observed between the two peptides. In previous studies, however, the neuritogenesis potency of TNP and HNP has been shown to surpass the potency of SV NGF in PC-12 cells [1-3] or natural polyphenols such as curcumin and resveratrol [21]. Compared to synthetic tripeptide (p-BTX-I) synthesized from *Bothrops atrox* venom [40], TNP and HNP were almost equal in their neuritogenesis potency. The reported differences in neuritogenesis potency may be due to the different experimental conditions

(i.e., doses, incubation time, etc.). As mentioned, mammalian NGF and snake venom NGF-induced TrkA dimerization activate MAPK and PI3K/AKT pathway-dependent neuritogenesis [1-3,15]. The selective inhibition of the MAPK and PI3K/AKT pathways by U0126 and LY294002 inhibitors, respectively, provides convincing evidence of the similarity of the custom peptides to snake venom NGF molecules [1-3,11]. The custom peptides we developed also activate the MAPK and PI3K/AKT signalling pathways for neuronal survival and differentiation in PC-12 cells [1-3,22,23]. In this study, we also reported that the custom peptides lacked cytotoxicity against different cell types and did not interfere with the mammalian blood coagulation cascade, indicating a lack of side effects based on *in vitro* experiments.

A plethora of studies have reported that the pathogenesis of PD is related to oxidative stress, resulting from a homeostatic imbalance in pro-oxidant and antioxidant genes that leads to the production of excessive ROS (free radicals), which ultimately triggers apoptotic cell death [24,25]. Some non-selective herbicides (such as PT) that are frequently used by farmers in agricultural practice, cause neurotoxicity and mitochondrial toxicity and can lead to the development of PD-like pathologies [26,27]. This study showed the neuroprotective potency of custom peptides TNP and HNP (pre-treatment conditions) in PC-12 cells by 15-20%. However, scrambled peptide under identical treatment conditions did not show neuroprotective activity. Therefore, we do not consider scrambled peptide for further studies. Further, their neuroprotective potency of custom peptides at a low concentration (100 ng/mL) and less incubation time (1h) suggest that these custom peptides may have a higher effect at low concentrations compared to other natural compounds [73, 77-79]. Our data also showed that both custom peptides possess similar neuroprotective effects but surpass the neuroprotective activity of mouse 2.5S-NGF (positive control) when tested at the same experimental conditions.

The antioxidant system against ROS is in dynamic balance under normal circumstances. PT induces an increase in ROS production, oxidative stress response, mitochondrial membrane potential, induction of apoptosis, and a reduced proliferation of PC-12 cells [28,29]. Studies have already reported that natural compounds such as naringin, curcumin, resveratrol, silymarin, pirfenidone, quercetin, selenium, bacosides, and Vitamin C have a significant therapeutic potential for treating PT-induced toxicity

[21,30-32]. Like these natural compounds, the custom peptides that we tested in this study have profound neuroprotective activity, and we aimed to investigate their mechanism of action. Following the findings from previous studies [29], we showed that PT treatment increases ROS production, and the custom peptide pre-treatment significantly attenuated the PT-induced ROS production, at a concentration (100 ng/mL, equivalent to 71 nM) that was 1,000 times less than that of Vitamin C (positive control, 10000 ng/mL). Although Vitamin C in this study showed appreciable antioxidant activity, it did not offer protection against PT-induced neurotoxicity. This suggests that antioxidant property alone may not be sufficient to offer protection against PT-induced neuronal damage and justifies the therapeutic application of the custom peptides under study. Additional quantitative proteomic analyses demonstrated the upregulation (fold-change increase) of antioxidant proteins such as heat shock protein 90 (hsp90), peroxiredoxin (prdx4), and glutamate dehydrogenase (glud1) in PT-treated PC-12 cells. These genes are reported to play an important role in the oxidative deamination and reduction of free radicals [33,34]. The increased ROS production in the PT group was validated by the upregulation of antioxidant proteins, and the activity of the custom peptides to attenuate the ROS production was confirmed by the downregulation of the same proteins in the PHNP group.

Mitochondrial dysfunction is another crucial phenomenon involved in the pathogenesis of PD, which is caused by oxidative stress [25,35]. Oxidative stress eventually leads to the loss of MMP, which results in the release of cytochrome C (pro-apoptotic protein) from the mitochondria and activation of the caspase cascade that induces cellular apoptosis [28,29,36,37]. Studies have shown that preventing mitochondrial dysfunction may be a therapeutic strategy for avoiding cell death [38]. In this study, we showed that pre-treatment of PC-12 cells with custom peptides significantly restored the depolarization of PT-induced MMP, which points to the neuroprotective property of custom peptides to maintain mitochondrial health and balance the expression of apoptotic proteins.

Due to the high energy demand of neuronal cells, they can be vulnerable to extensive mitochondrial damage, which can lead to nerve cell injury and death [38]. Different cellular pathways are involved in maintaining mitochondrial homeostasis and integrity, like the rapid translation of mitochondrial protein, pathways involved in

autophagy, energy (ATP) production via oxidative phosphorylation, amino acid synthesis, fat metabolism, and other biochemical pathways [25,39]. Together, these pathways maintain mitochondrial homeostasis by replacing defective mitochondria with new organelles that subsequently prevent neurodegeneration and show neuroprotective effects [40].

The proteomic analyses indicated that HNP pre-treatment restored the PT-induced upregulated genes and proteins involved in mitochondrial stress response pathways, such as glutamate dehydrogenase 1 (glud1) and glutamic-oxaloacetic transaminase (got2) involved in the mitochondrial redox balance [34,41]. To help maintain cellular integrity, HNP pre-treatment restored the upregulation of pro-apoptotic proteins in the PT group, such as cytochrome C (cyt-C), heat shock protein 60 (hspd1, GO:0043065), heat shock protein 70 (hspa5, GO:1903265). These proteins are reported to participate in the mitogen-activated protein kinase (p38/MAPK) signaling pathways, which are coupled to the oxidative stress response [42]. The global proteomic studies of snake venom NGF treated PC-12 cells had revealed about the oxidative stress-mediated apoptosis [1-3]. Moreover, the release of mitochondrial cyt-C into the cytoplasm in response to pro-apoptotic signals (bax, bid) and the activation of caspase-3 (cas-3) leads to apoptotic cell death [43-45]. In this study, the qRT-PCR analysis showed the downregulation of anti-apoptotic gene (bcl-2) expression and the upregulation of pro-apoptotic genes (cyt-C, bax, bid, hsp-70, and cas-3) in PT-treated PC-12 cells, which triggered cell death. The custom peptide pre-treatment restored the gene expression of the pro-/anti-apoptotic genes suggesting the therapeutic potency of the peptides to prevent PT-induced premature apoptosis in PC-12 cells.

The PT group of cells also showed upregulation of genes involved in detoxification (myh9 and ctsb) [46,47], the TCA cycle (cox5a and uqcrc2) [48,49] and the innate immune response (anxa1) [50], which were downregulated in the PHNP group of cells. As mentioned before, more energy is required to maintain mitochondria against oxidative stress, so the upregulation of these proteins is essential for the neuroprotective effect [38]. Our findings also suggest the upregulation of proteins involved in energy production by ATP synthesis via oxidative phosphorylation, such as the ATP synthase F1 subunit beta, alpha (atp5f1b and atp5f1a) [51] in HNP pre-treated cells, compared to the

PT group of cells. In addition, HNP pre-treatment showed a neuroprotective effect by counteracting the PT-induced downregulation of proteins directly or indirectly involved in neural development (myh10 and vim) and neuritogenesis [52] (gper1, cmkrl2, gper, gpr30, and gpr41) [52] (GO:0007399, GO:0019228).

A molecular network was constructed to show the multiple pathways that are interconnected and involved in HNP-mediated neuroprotection. Based on our experimental results, an overall neuroprotective mechanism was proposed for the action of the custom peptides against PT-induced neuronal damage (Fig 4.20).

Bibliography

[1] Islam, T., Majumder, M., Bidkar, A., Ghosh, S. S., Mukhopadhyay, R., Utkin, Y., and Mukherjee, A. K. Nerve growth factor from Indian Russell's viper venom (RVV-NGFa) shows high affinity binding to TrkA receptor expressed in breast cancer cells: Application of fluorescence labeled RVV-NGFa in the clinical diagnosis of breast cancer. *Biochimie*, 176: 31-44, 2020.

[2] Islam, T., Majumder, M., Kalita, B., Bhattacharjee, A., Mukhopadhyay, R., and Mukherjee, A. K. Transcriptomic, proteomic, and biochemical analyses reveal a novel neuritogenesis mechanism of *Naja naja* venom α-elapitoxin post binding to TrkA receptor of rat pheochromocytoma cells. *Journal of neurochemistry*, 155(6): 612-637, 2020.

[3] Islam, T., Madhubala, D., Mukhopadhyay, R., and Mukherjee, A. K. Transcriptomic and functional proteomics analyses to unveil the common and unique pathway (s) of neuritogenesis induced by Russell's viper venom nerve growth factor in rat pheochromocytoma neuronal cells. *Expert Review of Proteomics*, 18(6): 463-481, 2021.

[4] Schengrund, C.-L. Gangliosides: glycosphingolipids essential for normal neural development and function. *Trends in biochemical sciences*, 40(7): 397-406, 2015.

[5] Maliartchouk, S., Feng, Y., Ivanisevic, L., Debeir, T., Cuello, A. C., Burgess, K., and Saragovi, H. U. A designed peptidomimetic agonistic ligand of TrkA nerve growth factor receptors. *Molecular pharmacology*, 57(2): 385-391, 2000.

[6] Longo, F. M., Yang, T., Knowles, J. K., Xie, Y., Moore, L. A., and Massa, S. M. Small molecule neurotrophin receptor ligands: novel strategies for targeting Alzheimer's disease mechanisms. *Current Alzheimer Research*, 4(5): 503-506, 2007.

[7] Colangelo, A. M., Bianco, M. R., Vitagliano, L., Cavaliere, C., Cirillo, G., De Gioia, L., Diana, D., Colombo, D., Redaelli, C., and Zaccaro, L. A new nerve growth factor-mimetic peptide active on neuropathic pain in rats. *Journal of Neuroscience*, 28(11): 2698-2709, 2008.

[8] Gudasheva, T. A., Povarnina, P., Tarasiuk, A. V., and Seredenin, S. B. The low molecular weight brain-derived neurotrophic factor mimetics with antidepressant-like activity. *Current Pharmaceutical Design*, 25(6): 729-737, 2019.

[9] Muttenthaler, M., King, G. F., Adams, D. J., and Alewood, P. F. Trends in peptide drug discovery. *Nature reviews Drug discovery*, 20(4): 309-325, 2021.

[10] Longo, F. M. and Massa, S. M. Small-molecule modulation of neurotrophin receptors: a strategy for the treatment of neurological disease. *Nature reviews Drug discovery*, 12(7): 507-525, 2013.

[11] Bernardes, C. P., Santos, N. A., Sisti, F. M., Ferreira, R. S., Santos-Filho, N. A., Cintra, A. C., Cilli, E. M., Sampaio, S. V., and Santos, A. C. A synthetic snake-venom-based tripeptide (Glu-Val-Trp) protects PC12 cells from MPP+ toxicity by activating the NGF-signaling pathway. *Peptides*, 104: 24-34, 2018.

[12] Deshpande, R. R., Tiwari, A. P., Nyayanit, N., and Modak, M. In silico molecular docking analysis for repurposing therapeutics against multiple proteins from SARS-CoV-2. *European journal of pharmacology*, 886: 173430, 2020.

[13] Sarkar, I., Sen, G., Bhattacharya, M., Bhattacharyya, S., and Sen, A. In silico inquest reveals the efficacy of Cannabis in the treatment of post-Covid-19 related neurodegeneration. *Journal of Biomolecular Structure Dynamics*: 1-10, 2021.

[14] Kvetkina, A., Pislyagin, E., Menchinskaya, E., Yurchenko, E., Kalina, R., Kozlovskiy, S., Kaluzhskiy, L., Menshov, A., Kim, N., and Peigneur, S. Kunitz-Type Peptides from Sea Anemones Protect Neuronal Cells against Parkinson's Disease Inductors via Inhibition of ROS Production and ATP-Induced P2X7 Receptor Activation. *International Journal of Molecular Sciences*, 23(9): 5115, 2022.

[15] Wehrman, T., He, X., Raab, B., Dukipatti, A., Blau, H., and Garcia, K. C. Structural and mechanistic insights into nerve growth factor interactions with the TrkA and p75 receptors. *Neuron*, 53(1): 25-38, 2007.

[16] Klein, R., Jing, S., Nanduri, V., O'Rourke, E., and Barbacid, M. The trk proto-oncogene encodes a receptor for nerve growth factor. *Cell*, 65(1): 189-197, 1991.

[17] Benedetti, M., Levi, A., and Chao, M. V. Differential expression of nerve growth factor receptors leads to altered binding affinity and neurotrophin responsiveness. *Proceedings of the National Academy of Sciences*, 90(16): 7859-7863, 1993.

[18] Kalvala, A. K., Yerra, V. G., and Kumar, A. LONP1 induction by SRT1720 attenuates mitochondrial dysfunction against high glucose induced neurotoxicity in PC12 cells. *Toxicology in vitro*, 62: 104695, 2020.

[19] Zhang, L., Dong, M.-N., Deng, J., Zhang, C.-H., and Liu, M.-W. Resveratrol exhibits neuroprotection against paraquat-induced PC12 cells via heme oxygenase 1 upregulation by decreasing MiR-136-5p expression. *Bioengineered*, 13(3): 7065-7081, 2022.

[20] Grumolato, L., Louiset, E., Alexandre, D., Aït-Ali, D., Turquier, V., Fournier, A., Fasolo, A., Vaudry, H., and Anouar, Y. PACAP and NGF regulate common and distinct traits of the sympathoadrenal lineage: effects on electrical properties, gene markers and transcription factors in differentiating PC12 cells. *European Journal of Neuroscience*, 17(1): 71-82, 2003.

[21] Bora-Tatar, G. and Erdem-Yurter, H. Investigations of curcumin and resveratrol on neurite outgrowth: perspectives on spinal muscular atrophy. *BioMed Research International*, 2014, 2014.

[22] Reichardt, L. F. Neurotrophin-regulated signalling pathways. *Philosophical Transactions of the Royal Society B: Biological Sciences*, 361(1473): 1545-1564, 2006.

[23] Skaper, S. D. The biology of neurotrophins, signalling pathways, and functional peptide mimetics of neurotrophins and their receptors. *CNS Neurological Disorders-Drug Targets*, 7(1): 46-62, 2008.

[24] Barnham, K. J., Masters, C. L., and Bush, A. I. Neurodegenerative diseases and oxidative stress. *Nature reviews Drug discovery*, 3(3): 205-214, 2004.

[25] Areti, A., Komirishetty, P., Akuthota, M., Malik, R. A., and Kumar, A. Melatonin prevents mitochondrial dysfunction and promotes neuroprotection by inducing autophagy during oxaliplatin-evoked peripheral neuropathy. *Journal of Pineal Research*, 62(3): e12393, 2017.

[26] Bora, S., Vardhan, G. S. H., Deka, N., Khataniar, L., Gogoi, D., and Baruah, A. Paraquat exposure over generation affects lifespan and reproduction through mitochondrial disruption in C. elegans. *Toxicology*, 447: 152632, 2021.

[27] Bastías-Candia, S., Zolezzi, J. M., and Inestrosa, N. C. Revisiting the paraquat-induced sporadic Parkinson's disease-like model. *Molecular Neurobiology*, 56(2): 1044-1055, 2019.

[28] Lee, P.-C., Bordelon, Y., Bronstein, J., and Ritz, B. Traumatic brain injury, paraquat exposure, and their relationship to Parkinson disease. *Neurology India*, 79(20): 2061-2066, 2012.

[29] Zhang, Z.-D., Yang, Y.-J., Qin, Z., Liu, X.-W., Li, S.-H., Bai, L.-X., and Li, J.-Y. Protective Activity of Aspirin Eugenol Ester on Paraquat-Induced Cell Damage in SH-SY5Y Cells. *Oxidative Medicine Cellular Longevity*, 2021, 2021.

[30] Blanco-Ayala, T., Andérica-Romero, A., and Pedraza-Chaverri, J. New insights into antioxidant strategies against paraquat toxicity. *Free Radical Research*, 48(6): 623-640, 2014.

[31] Jia, W., Su, Q., Cheng, Q., Peng, Q., Qiao, A., Luo, X., Zhang, J., and Wang, Y. Neuroprotective Effects of Palmatine via the Enhancement of Antioxidant Defense and Small Heat Shock Protein Expression in Aβ-Transgenic *Caenorhabditis elegans*. *Oxidative Medicine Cellular Longevity*, 2021:9966223, 2021.

[32] Hou, R. R., Chen, J. Z., Chen, H., Kang, X. G., Li, M. G., and Wang, B. R. Neuroprotective effects of (-)-epigallocatechin-3-gallate (EGCG) on paraquat-induced apoptosis in PC12 cells. *Cell Biol Int*, 32(1): 22-30, 2008. 10.1016/j.cellbi.2007.08.007

[33] Jin, D.-Y., Chae, H. Z., Rhee, S. G., and Jeang, K.-T. Regulatory role for a novel human thioredoxin peroxidase in NF-κB activation. *Journal of biological chemistry*, 272(49): 30952-30961, 1997.

[34] Zhang, X., Vincent, A. S., Halliwell, B., and Wong, K. P. A mechanism of sulfite neurotoxicity: direct inhibition of glutamate dehydrogenase. *Journal Of Biological Chemistry*, 279(41): 43035-43045, 2004.

[35] Yamaguchi, A., Ishikawa, K. I., Inoshita, T., Shiba-Fukushima, K., Saiki, S., Hatano, T., Mori, A., Oji, Y., Okuzumi, A., Li, Y., Funayama, M., Imai, Y., Hattori, N., and Akamatsu, W. Identifying Therapeutic Agents for Amelioration of Mitochondrial Clearance Disorder in Neurons of Familial Parkinson Disease. *Stem Cell Reports*, 14(6): 1060-1075, 2020. 10.1016/j.stemcr.2020.04.011

[36] Yang, W. and Tiffany-Castiglioni, E. Paraquat-induced apoptosis in human neuroblastoma SH-SY5Y cells: involvement of p53 and mitochondria. *Journal of Toxicology Environmental Health, Part A*, 71(4): 289-299, 2008.

[37] Islam, M. T. Oxidative stress and mitochondrial dysfunction-linked neurodegenerative disorders. *Neurological Research*, 39(1): 73-82, 2017.

[38] Golpich, M., Amini, E., Mohamed, Z., Azman Ali, R., Mohamed Ibrahim, N., and Ahmadiani, A. Mitochondrial dysfunction and biogenesis in neurodegenerative diseases: pathogenesis and treatment. *CNS Neuroscience Therapeutics*, 23(1): 5-22, 2017.

[39] Pagliarini, D. J., Calvo, S. E., Chang, B., Sheth, S. A., Vafai, S. B., Ong, S.-E., Walford, G. A., Sugiana, C., Boneh, A., and Chen, W. K. A mitochondrial protein compendium elucidates complex I disease biology. *Cell*, 134(1): 112-123, 2008.

[40] Okamoto, K. and Kondo-Okamoto, N. Mitochondria and autophagy: critical interplay between the two homeostats. *Biochimica et Biophysica Acta -General Subjects*, 1820(5): 595-600, 2012.

[41] Guidetti, P., Amori, L., Sapko, M. T., Okuno, E., and Schwarcz, R. Mitochondrial aspartate aminotransferase: a third kynurenate-producing enzyme in the mammalian brain. *Journal of Neurochemistry*, 102(1): 103-111, 2007.

[42] Song, Y., Liang, X., Hu, Y., Wang, Y., Yu, H., and Yang, K. p, p′-DDE induces mitochondria-mediated apoptosis of cultured rat Sertoli cells. *Toxicology*, 253(1-3): 53-61, 2008.

[43] Mukherjee, A. K., Saviola, A. J., Burns, P. D., and Mackessy, S. P. Apoptosis induction in human breast cancer (MCF-7) cells by a novel venom L-amino acid oxidase (Rusvinoxidase) is independent of its enzymatic activity and is accompanied by caspase-7 activation and reactive oxygen species production. *Apoptosis*, 20(10): 1358-1372, 2015.

[44] Thakur, R., Kini, S., Kurkalang, S., Banerjee, A., Chatterjee, P., Chanda, A., Chatterjee, A., Panda, D., and Mukherjee, A. K. Mechanism of apoptosis induction in human breast cancer MCF-7 cell by Ruviprase, a small peptide from *Daboia russelii russelii* venom. *Chemico-Biological Interactions*, 258: 297-304, 2016.

[45] Sanphui, P., Pramanik, S. K., Chatterjee, N., Moorthi, P., Banerji, B., and Biswas, S. C. Efficacy of cyclin dependent kinase 4 inhibitors as potent neuroprotective agents against insults relevant to Alzheimer's disease. *PloS One*, 8(11): e78842, 2013.

[46] Ozaslan, D., Wang, S., Ahmed, B. A., Kocabas, A. M., McCastlain, J. C., Bene, A., and Kilic, F. Glycosyl modification facilitates homo-and hetero-oligomerization of the serotonin transporter: a specific role for sialic acid residues. *Journal Of Biological Chemistry*, 278(45): 43991-44000, 2003.

[47] Wen, Y.-D., Sheng, R., Zhang, L.-S., Han, R., Zhang, X., Zhang, X.-D., Han, F., Fukunaga, K., and Qin, Z.-H. Neuronal injury in rat model of permanent focal cerebral ischemia is associated with activation of autophagic and lysosomal pathways. *Autophagy*, 4(6): 762-769, 2008.

[48] Schägger, H., Noack, H., Halangk, W., Brandt, U., and Von Jagow, G. Cytochrome-c Oxidase in Developing Rat Heart Enzymic Properties and Amino-terminal Sequences Suggest Identity of the Fetal Heart and the Adult Liver Isoform. *European Journal Of Biochemistry*, 230(1): 235-241, 1995.

[49] Sun, G., Kinter, M. T., and Anderson, V. E. Mass spectrometric characterization of mitochondrial electron transport complexes: subunits of the rat heart ubiquinol–cytochrome c reductase. *Journal Of Mass Spectrometry*, 38(5): 531-539, 2003.

[50] De, B. K., Misono, K. S., Lukas, T., Mroczkowski, B., and Cohen, S. A calcium-dependent 35-kilodalton substrate for epidermal growth factor receptor/kinase isolated from normal tissue. *Journal Of Biological Chemistry*, 261(29): 13784-13792, 1986.

[51] Pedersen, P. L., Williams, N., and Hullihen, J. Mitochondrial ATP synthase: dramatic magnesium-induced alterations in the structure and function of the F1-ATPase moiety. *Biochemistry*, 26(26): 8631-8637, 1987.

[52] Xu, H., Qin, S., Carrasco, G., Dai, Y., Filardo, E., Prossnitz, E., Battaglia, G., Doncarlos, L., and Muma, N. Extra-nuclear estrogen receptor GPR30 regulates serotonin function in rat hypothalamus. *Neuroscience*, 158(4): 1599-1607, 2009.